JOURNAL OF GEOPHYSICAL RESEARCH, VOL. 91, NO. B7, PAGES 7241–7260, JUNE 10, 1986

Coupled Free Oscillations of an Aspherical, Dissipative, Rotating Earth: Galerkin Theory

JEFFREY PARK[1] AND FREEMAN GILBERT

Institute of Geophysics and Planetary Physics, Scripps Institution of Oceanography, University of California, San Diego

Variational theory based on self-adjoint equations of motion cannot fully represent the interaction of the earth's seismic free oscillations in the presence of lateral structure, attenuation, and rotation. The more general Galerkin procedure can model correctly the frequencies and attenuation rates of hybrid oscillations. Implementation of either algorithm leads to a generalized matrix eigenvalue problem in which the potential and kinetic energy interactions are separated into distinct matrices. The interaction of the earth's seismic free oscillations due to aspherical structure, attenuation, and rotation is best treated as a matrix eigenvalue problem. The presence of attenuation causes the matrices to be non-Hermitian and requires the use of a general Galerkin procedure. Physical dispersion, represented as a logarithmic function in frequency, must be represented by a truncated Taylor series about a fiducial frequency in order to be incorporated in the Galerkin formalism in a numerically tractable manner. The earth's rotation introduces an interaction matrix distinct from the potential and kinetic energy matrices, leading to a quadratic eigenvalue problem. A simple approximation leads to an eigenvalue problem linear in squared frequency. Tests show that this approximation is accurate for calculations using modes of frequencies $f \geq 1$ mHz, unless interaction across a wide frequency band is modeled. Hybrid oscillation particle motions are represented by matrix eigenvectors that can be significantly nonorthogonal. The degrees of freedom in the low-frequency seismic system remain distinct, since source excitation is calculated by using dual eigenvectors. Synthetic seismograms that are constructed from Galerkin coupling calculations without reference to this eigenvector nonorthogonality can be disastrously noncausal.

1. INTRODUCTION

The evidence for significant lateral structure throughout the mantle grows with each round of observational studies in low-frequency seismology. Each of these studies relies on some simplification of the full equations of seismic motion. Lateral models derived from time domain observations of surface waves [*Okal, 1977; Nakanishi and Anderson*, 1983, 1984; *Woodhouse and Dziewonski*, 1984; *Tanimoto*, 1984; *Tanimoto and Anderson*, 1985] rely on a high-frequency, geometric ray approximation to the equations of motion, often termed the great circle approximation. The limitations of this approximation for surface waves are best suggested by the study of *Woodhouse and Girnius* [1982], which presents kernels for offpath scattering. Moreover, both body wave and surface wave studies thus far have used tomographic (fixed ray) approximations to the geometric ray formulation. The shortcomings of this tomographic approximation for surface waves have been demonstrated by *Lay and Kanamori* [1985] and *Wong and Woodhouse* [1983]. Both noted a significant lateral wander of the "true" geometric ray from the tomographic approximation. Lateral models constructed using apparent frequency shifts of fundamental spheroidal free oscillations [*Silver and Jordan*, 1981; *Masters et al.*, 1982] use an asymptotic representation of the effect of the first-order splitting of the singlets of degenerate free oscillation multiplets due to *Jordan* [1978], that at bottom, also relies on a tomographic (i.e., great circle) approximation to the equations of motion. Spheroidal overtone splitting observations [*Masters and Gilbert*, 1981; M. Ritzwoller *et al.*, unpublished manuscript, 1986] have often appeared to be characterized by simple spherical harmonic surface dependence. Although this behavior is a blessing so far as observing isolated singlets is concerned, it restricts our inferential capability to only axisymmetric models (i.e., spherical harmonic expansions with azimuthal order $t = 0$).

Although a bootstrap-style iterative improvement in lateral structure models using successively refined representations of the full equations of motion is virtually inevitable, it has become both possible and feasible to model complete low-frequency seismograms using sums of coupled free oscillations. The approximations that must be made in such calculations in return for numerical tractability are different in nature from those associated with the high-frequency, geometric ray approximation. A first-order splitting calculation, in which no coupling is assumed between distinct free oscillation multiplets, is the first-order approximation to the full coupled mode seismogram and can represent much more wave propagation behavior than the great circle surface wave approximation. The effect of including interactions between some modes and neglecting interactions between others can be assessed numerically using theorems from matrix algebra. Although an inversion scheme using the full coupled mode seismogram formalism has not yet been attempted, we can compute seismograms for realistic models to discover more accurately the behavior of low-frequency seismic waves in a laterally variable earth.

The goal of this study is to show how free oscillation coupling calculations can be incorporated into our search for global lateral structure in the deep earth. A discussion

[1]Now at Geophysical Fluid Dynamics Program, Princeton University, Princeton, New Jersey.

Paper number 5B5475.
0148-0227/86/005B-5475$05.00

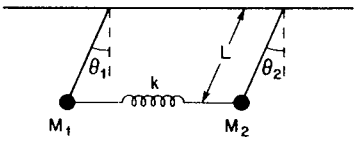

Fig. 1. Schematic of coupled pendulum problem discussed in text.

of the methods of performing coupling calculations is given, followed by recipes and examples of the construction of synthetic seismograms. Examples of coupling due to rotational Coriolis force that are clearly observable have been given by *Masters et al.* [1983] and *Park* [1986] and were shown to correspond to coupling calculations in a qualitative manner. The discussion of coupling kernels, whose form will determine our ability to resolve structure, will be addressed in a later study. Various degrees of coupling interaction are demonstrated and compared in coupled, fundamental mode, synthetic seismograms.

We preface the theoretical exposition with section 2, where the mechanical problem of two coupled pendula is examined. In this example we model the coupling and attenuation properties of the system in a manner identical to that later applied in free oscillation problems. The reader can inspect how the relations of matrix algebra apply to the physical problem of excitation and attenuation properties.

Section 3 outlines the Galerkin formalism for calculating coupled modes from a fixed basis Lagrangian interaction. Formulae for source excitation calculations are also given in a recipe for constructing coupled mode synthetic seismograms. The equations of motion for a rotating earth lead properly to a quadratic eigenvalue problem. The inclusion of physical dispersion into the eigenproblem will, in the case of an absorption band attenuation model, lead to a transcendental eigenvalue problem. Nearly all applications can be adequately modeled as a quadratic eigenvalue problem. We show how the quadratic eigenvalue problem reduces to a more tractable linear eigenvalue problem using an approximation to the term linear in oscillation frequency ω.

Section 4 discusses the numerical effects of adding dissipation to the problem. If spherical earth modal singlets with differing attenuation rates are included in a coupling calculation, the matrix interaction system loses its symmetry. This increases the numerical computations required for solution by a factor of 3 or more. The nonorthogonality of distinct-frequency free oscillation particle motions in the presence of attenuation is an additional nontrivial consequence.

Sections 5 and 6 present numerical examples of coupling interaction on rotating, attenuative, earth models with lateral structure. Section 5 examines the numerical error introduced by solving the Galerkin interaction problem with a linear eigenvalue problem rather than the more accurate quadratic eigenvalue formalism. The discrepancy is found to be small but should be detectable for the gravest free oscillations. Section 6 shows examples of how the non-Hermiticity of the attenuative interaction matrices leads to significant nonorthogonality of free oscillation modal singlets. We show how, if this nonorthogonality is neglected when calculating synthetic seismograms, severe problems (e.g., noncausal seismic motions) can result.

2. A Simple Mechanical Example

We illustrate the importance of dissipation in coupling problems with a simple mechanical example. Suppose we have two pendula (Figure 1) with identical length L side by side with inertial masses M_1, M_2, where $M_1 \approx M_2$. The two pendula are connected with a massless spring of spring constant k. The angle θ_i represents the deflection of the ith pendulum small enough to approximate $\sin\theta_i \approx \theta_i$. We can immediately write down the Lagrangian energy functions for potential and kinetic energy, respectively;

$$V = \tfrac{1}{2}M_1gL\theta_1^2 + \tfrac{1}{2}M_2gL\theta_2^2 + \tfrac{1}{2}kL^2(\theta_1-\theta_2)^2$$
$$T = \tfrac{1}{2}M_1L^2\left(\frac{d\theta_1}{dt}\right)^2 + \tfrac{1}{2}M_2L^2\left(\frac{d\theta_2}{dt}\right)^2 \tag{1}$$

where g is gravity. We assume sinusoidal oscillation with frequency ω and obtain a 2×2 generalized eigenvalue problem

$$\det\left\{\begin{bmatrix} M_1gL+kL^2 & -kL^2 \\ -kL^2 & M_2gL+kL^2\end{bmatrix} - \omega^2\begin{bmatrix} M_1L^2 & 0 \\ 0 & M_2L^2\end{bmatrix}\right\} = 0 \tag{2}$$

The most efficient mathematical solution of (2) proceeds by diagonalizing the kinetic energy interaction matrix to obtain a standard eigenvalue problem:

$$\det\left\{\begin{bmatrix} \frac{g}{L}+\frac{k}{M_1} & \frac{-k}{(M_1M_2)^{1/2}} \\ \frac{-k}{(M_1M_2)^{1/2}} & \frac{g}{L}+\frac{k}{M_2}\end{bmatrix} - \omega^2\begin{bmatrix} 1 & 0 \\ 0 & 1\end{bmatrix}\right\} = 0 \tag{3}$$

If $k = 0$ we obtain $\omega = \sqrt{g/L}$ for both (uncoupled) modes of vibration. If $k > 0$, $\omega = \sqrt{g/L}$, $\{(g/L)+k[(1/M_1)+(1/M_2)]\}^{1/2}$ are the split doublet frequencies. The splitting width increases monotonically with increasing k. This behavior is well known from mechanical coupling problems [*Sommerfeld*, 1952, pp. 106–111]. The orthonormal eigenvectors of (3) are

$$\tilde{\boldsymbol{\alpha}}_- = (M_2^{-1/2}, M_1^{-1/2})/(M_1+M_2)^{1/2}$$

and

$$\tilde{\boldsymbol{\alpha}}_+ = (M_1^{-1/2}, -M_2^{-1/2})/(M_1+M_2)^{1/2}$$

These vector quantities must be transformed to the eigenvectors $\boldsymbol{\alpha}_+, \boldsymbol{\alpha}_-$ of the original physical problem (2). $\boldsymbol{\alpha}_- = 2^{-1/2}(1,1)$, $\boldsymbol{\alpha}_+ = (M_2,-M_1)/(M_1^2+M_2^2)^{1/2}$ are the free modes of oscillation of the coupled pendulum system. The two solutions $\boldsymbol{\alpha}_-$, $\boldsymbol{\alpha}_+$ refer to modes that leave the spring undisturbed and flex it, respectively. Note that $\boldsymbol{\alpha}_- \cdot \boldsymbol{\alpha}_+ \neq 0$ unless $M_1 = M_2$. The two modes of motion are orthogonal, however, when the kinetic energy metric defines the inner product. (This is the usual requirement for the modes to be "orthogonal" in the physical sense.)

The nonorthogonality of these vector representations of free mode displacements can cause some confusion in evaluating pendulum motion from given initial displacement values $\theta_1^{(0)}$ and $\theta_2^{(0)}$. For $\theta_1^{(0)} = \theta_2^{(0)}$, examination of the equations of motion for the system reveals that $\theta_1(t) = \theta_2(t)$ for all succeeding times. This is true only if

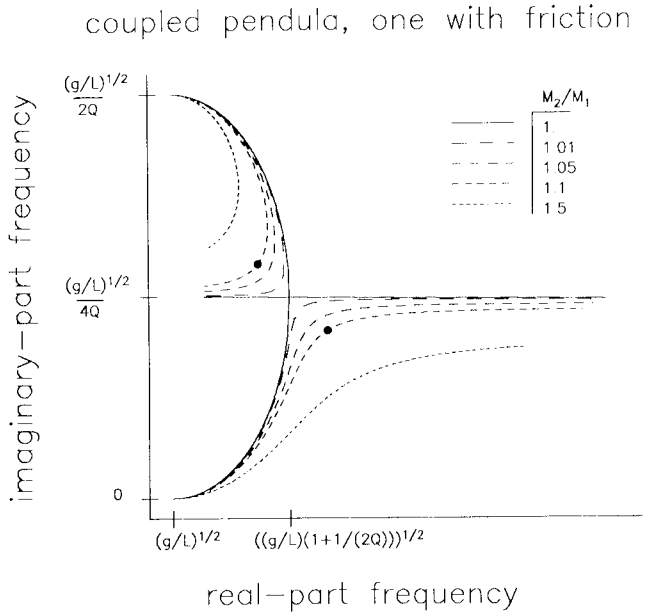

Fig. 2. Each line represents a locus of $(\mathrm{Re}(\omega),\mathrm{Im}(\omega))$ values as a function of spring constant k. At $k=0$, the two resonant frequencies are $\omega_- = \sqrt{g/L}$, $\omega_+ = \sqrt{g/L}\,(1+i(2Q)^{-1})$. As k increases, ω_- and ω_+ migrate to sweep out the curves shown, one set for each value of M_2/M_1. When $M_2 = M_1$, there is a critical value of k for which $\omega_+ = \omega_-$ and the displacement eigenvectors become parallel.

the mode $\boldsymbol{\alpha}_+$ is not excited. The initial displacement $(\theta_1^{(0)},\theta_2^{(0)})$ is parallel to $\boldsymbol{\alpha}_-$ but not orthogonal to $\boldsymbol{\alpha}_+$ and therefore is an improper quantity with which to calculate modal excitation. In seismic excitation problems, fault displacement is usually expressed in terms of "equivalent forces," the force field required to suspend fault motion until rupture occurs. The force vector required to suspend the initial displacement $(\theta_1^{(0)},\theta_2^{(0)})$ is $\mathbf{f}^{(0)} = (M_1 g\theta_1^{(0)}, M_2 g\theta_2^{(0)})$. If $\theta_1^{(0)} = \theta_2^{(0)}$, $\mathbf{f}^{(0)} \cdot \boldsymbol{\alpha}_+ = 0$ and the desired orthogonality is achieved. In the excitation of pendulum motion the displacement $\boldsymbol{\alpha}_\pm$ must be multiplied by equivalent force vectors. Note that this requirement is mathematically equivalent to the orthogonality of modal displacement with respect to the kinetic energy inner product (the right-hand matrix in (2)). The "equivalent force" metaphor, however, is commonly used to describe seismic sources and so better to illustrate the connection between the pendulum example and the excitation of seismic free oscillations.

Suppose the first pendulum is supported on a frictionless hinge and the second one on a slightly rusty hinge. We can model the energy lost to dissipation in the second pendulum as a hysteresis effect in which it loses a fraction $2\pi/Q$ of its vibrational energy during each full oscillation. The parameter Q, assumed to be much larger than unity, is the quality factor. This model is uniformly preferred in seismic free oscillation studies over the velocity-dependent frictional potentials favored in most mechanics texts [e.g., *Goldstein*, 1980, p. 265], since seismic Q of free oscillations is directly measurable. The hysteresis attenuation is modeled by adding a small imaginary part to the frictionless pendulum frequency: $\omega^2 = (g/L)(1+iQ^{-1})$. Substitution of this expression into (2) yields a general complex eigenproblem that leads to squared eigenfrequencies

$$\omega_\pm^2 = \frac{g}{L}\left(1+\frac{i}{2Q}\right) + \tfrac{1}{2}\left(\frac{k}{M_1}+\frac{k}{M_2}\right) \pm \tfrac{1}{2}\left[\left(\frac{k}{M_1}+\frac{k}{M_2}\right)^2 - \frac{g^2}{Q^2L^2} + 2i\left(\frac{k}{M_2}-\frac{k}{M_1}\right)\frac{g}{LQ}\right]^{1/2} \quad (4)$$

The behavior of $\omega_\pm$ for $k \geq 0$ is plotted in Figure 2. Each line represents a locus of $\omega_\pm$ values for a given $r = M_2/M_1$. As k increases from zero, the two eigenfrequencies come closer, shaving the difference in squared eigenfrequency to a minimum as the imaginary-part (attenuative) frequency components become more equal. As $k \to \infty$, the difference between the imaginary components approaches an asymptotic minimum

$$\min(\mathrm{Im}(\omega_+ - \omega_-)) = \frac{g}{LQ}\left[\left(1-\frac{M_2}{M_1}\right) / \left(1+\frac{M_2}{M_1}\right)\right] \quad (5)$$

As k increases, the repulsion of the real-part eigenfrequencies takes over. For $M_2 = M_1$ this transition in behavior occurs sharply when the spring constant $k = (g/QL)\,[(1/M_1)+(1/M_2)]^{-1}$, at which point the eigenvalues are accidentally degenerate. The complicated attraction and repulsion of eigenvalues in the complex plane mimic the frequency behavior of coupled free oscillations with variable attenuation rates.

The pendulum motions in this example are very different from those appropriate to a frictionless system. In a frictionless system the ordinary complex vector dot product $\tilde{\boldsymbol{\alpha}}_+^* \cdot \tilde{\boldsymbol{\alpha}}_- = 0$. If one computes $|\tilde{\boldsymbol{\alpha}}_+^* \cdot \tilde{\boldsymbol{\alpha}}_-|$ as a function of k for the system with hysteresis friction, the degree of nonorthogonality is striking (Figure 3). This behavior makes necessary the introduction of dual eigenvectors to describe properly the forced motions of the system. This has been recognized in the free oscillation problem by *Dahlen* [1981] and is crucial to the construction of synthetic seismograms from coupled free oscillations of varying attenuation rates. The dual eigenvectors $\tilde{\boldsymbol{\beta}}_+, \tilde{\boldsymbol{\beta}}_-$ of this system are found by solving the "adjoint"

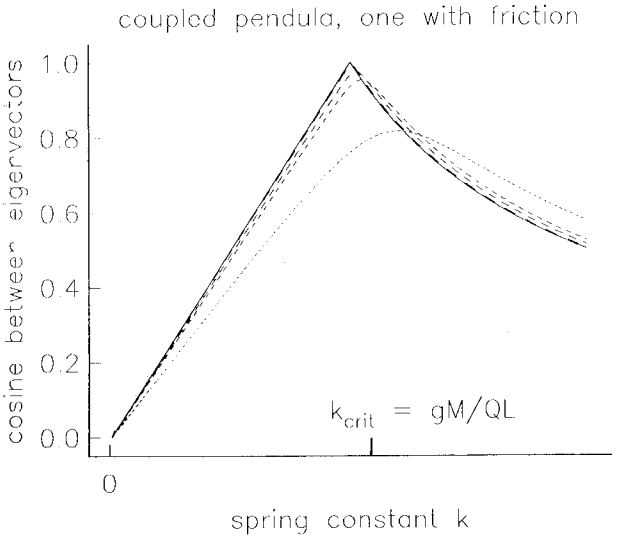

Fig. 3. Direction cosine between $\tilde{\boldsymbol{\alpha}}_+$ and $\tilde{\boldsymbol{\alpha}}_-$, defined by $\cos\xi = \tilde{\boldsymbol{\alpha}}_+^* \cdot \tilde{\boldsymbol{\alpha}}_- / (\|\tilde{\boldsymbol{\alpha}}_+\|\,\|\tilde{\boldsymbol{\alpha}}_-\|)^{1/2}$, plotted as a function of spring constant k for the choices of M_2/M_1 used in Figure 2. The value of k for which $\omega_+ = \omega_-$ when $M_1 = M_2$ is indicated along the spring constant ordinate.

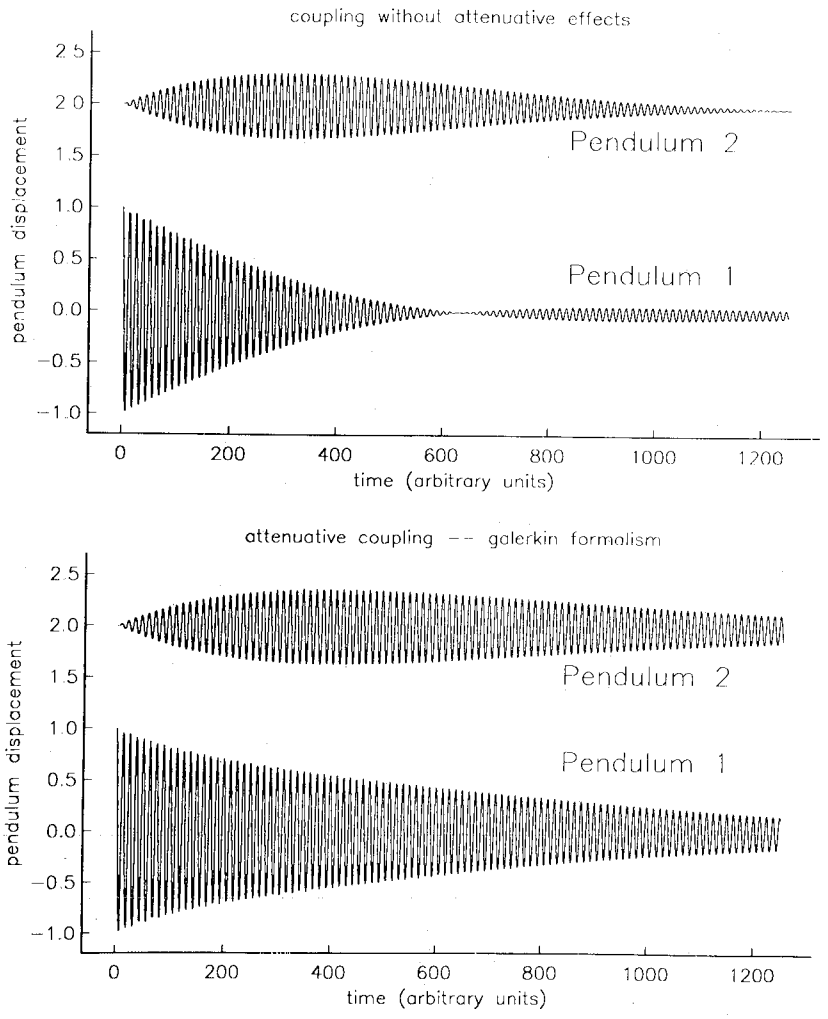

Fig. 4. Time series of pendulum motion for two coupling examples. The top two traces show motion of the two pendula coupled without reference to attenuation effects but with both free modes given $Q = 100$. The lower two traces show pendulum motion calculated with the Galerkin procedure, cognizant of attenuative coupling effects. The lower traces do not show the beating between pendula present in the upper traces.

eigenvector-eigenvalue problem. This problem is the transpose of (2). If the coupling interaction were nonattenuative, the matrix system would be real-valued symmetric or complex valued Hermitian. Solving the adjoint problem would give dual vectors $\tilde{\boldsymbol{\beta}}_\pm = \tilde{\boldsymbol{\alpha}}_\pm^* / \|\tilde{\alpha}_\pm\|^2$. If $\|\tilde{\alpha}_\pm\| = 1$, the dual vector formalism reduces to the ordinary complex-vector dot product. With friction, the matrices in (2) are complex-valued symmetric, and $\tilde{\boldsymbol{\beta}}_+ = \tilde{\boldsymbol{\alpha}}_+$ and $\tilde{\boldsymbol{\beta}}_- = \tilde{\boldsymbol{\alpha}}_-$ as long as we choose the complex scaling factor that forces $\tilde{\boldsymbol{\alpha}}_\pm \cdot \tilde{\boldsymbol{\alpha}}_\pm = 1$. Otherwise $\tilde{\boldsymbol{\beta}}_\pm = \tilde{\boldsymbol{\alpha}}_\pm / (\tilde{\boldsymbol{\alpha}}_\pm \cdot \tilde{\boldsymbol{\alpha}}_\pm)$.

Despite the "self-dual" appearance of the eigenvectors and their adjoints, they are not orthogonal under the properly defined Euclidean norm in complex two space, i.e., $\|\tilde{\boldsymbol{\alpha}}\| = \tilde{\boldsymbol{\alpha}}^* \cdot \tilde{\boldsymbol{\alpha}}$. In general, $\tilde{\boldsymbol{\beta}} \cdot \tilde{\boldsymbol{\alpha}} = 0$ does not imply $\tilde{\boldsymbol{\beta}}^* \cdot \tilde{\boldsymbol{\alpha}} = 0$ if the components of $\tilde{\boldsymbol{\beta}}$ and $\tilde{\boldsymbol{\alpha}}$ have nonzero relative phase. Nonzero relative phase means that in a given eigenmode, the two pendula do not swing either in tandem or in exact opposition. We can illustrate this with the time-dependent behavior of the coupled pendulum example. Let $g/L = 1\ \mathrm{s}^{-2}$, $Q = 50$, and $M_2/M_1 = r = 1.1$. We choose the spring constant $k = 0.01045\ M_1$, the value at which the squared eigenfrequencies $\omega_\pm^2$ are closest. The frequencies $\omega_\pm^2$ are indicated in Figure 2. The two free modes of oscillation have quality factors $Q_+ \cong 130$, $Q_- \cong 82.6$. The eigenvector solutions (unnormalized) are $\tilde{\alpha}_+ = (1., -0.166 + 0.779i)$, $\tilde{\alpha}_- \approx (1., 0.261 + 1.227i)$. The unnormalized displacement vectors $\boldsymbol{\alpha}_\pm$ for the free modes of oscillation are gotten by dividing the second component of $\tilde{\boldsymbol{\alpha}}_\pm$ by $\sqrt{r} \approx 1.05$. From the complex phase of the second component relative to the first, it is seen that in the positive mode, the motion of the first pendulum leads the motion of the second by roughly 102°. In the negative mode, the motion of the second pendulum lags behind that of the first by roughly 78°. This contrasts with the 0° and 180° phase lags of the nonattenuative coupling case. The splitting of real-part eigenfrequencies is roughly 5 times greater in the nonattenuative coupling case for this choice of parameters. To contrast the two coupling schemes (attenuative and nonattenuative), we give each nonattenuatively coupled free mode a Q of 100 and plot in Figure 4 the pendulum motion arising from unit initial displacement of the first pendulum for both coupling schemes. We plot motion for $0 < t < 1250$ s, correspond-

ing to roughly 200 cycles of motion. Note the beating between the two pendula in the nonattenuative coupling example. The beating, as explicated in many mechanics textbooks, has a modulation frequency $\omega_{\text{mod}} = \text{Re}(\omega_+ - \omega_-)$. Energy will pass back and forth between the pendula until all motion decays away. The motion of the attenuative coupling example is not visibly affected by beating. Two effects cause this. First, the modulation frequency $\omega_{\text{mod}} = \text{Re}(\omega_+ - \omega_-)$ for this example is much smaller. Second, the free modes have distinct attenuation rates. If both $\boldsymbol{\alpha}_+, \boldsymbol{\alpha}_-$ modes of oscillation are initially equally excited, the negative mode motion will have decayed to $\sim 25\%$ of the positive mode motion amplitude at the end of 100 cycles. Destructive interference cannot occur with the amplitudes so mismatched. As $t \rightarrow \infty$, the relative phase of the pendulum displacements will approach that between the components of $\boldsymbol{\alpha}_+$, with a steady ratio of amplitudes.

Many of the qualitative effects derived from this simple mechanical example will carry over into the description of the coupled seismic free oscillations of the earth. Although the mathematics involved is more complex, the coupling of spheroidal and toroidal seismic oscillations is formally similar to the above pendulum example. Especially when influenced by the rotational Coriolis force, spheroidal and toroidal modes couple and split in real-part frequencies, while tending to average the higher toroidal attenuation rate with the lower spheroidal attenuation. Residually higher Q of dominantly spheroidal (St) modes can prove troublesome in the search for dominantly toroidal (Ts) modes in seismic data. As in the coupled pendulum example, Ts motion can decay rapidly relative to the less dissipative St motion, obscuring its existence beyond the first few dozen oscillations. If the spatial component relative phase is known, it is possible in principle to remove the St motion via a matched filter. In practice, however, St motion is composed of dozens of distinct modes of oscillation, complicating any effort to remove it.

In order to discuss more fully the coupling of seismic free oscillations and its expression in both the frequency and time domains, it is necessary to introduce more sophisticated mathematics, in particular, the Galerkin formalism. The outline of this procedure is the subject of the next two sections.

3. Variational Theory: Nondissipative Earth Models

Before we outline the Galerkin procedure, it will be helpful briefly to review variational theory as applied to the earth's normal modes. The formal aspects of the normal mode variational principle have been developed in detail by others [e.g., *Dahlen*, 1973; *Woodhouse*, 1976; *Woodhouse and Dahlen*, 1978], and it is to those sources that the reader must turn for a full derivation. One begins with the equations of motion for small elastic-gravitational oscillations of an earth model about stable equilibrium. The earth model is contained within a volume V and is characterized by material and stress properties as a function of vector position $\mathbf{r}$ within V: density $\rho(\mathbf{r})$, gravitational potential $\phi(\mathbf{r})$, an initial stress field $\mathbf{T}_0(\mathbf{r})$, and a fourth-order tensor $\mathbf{C} = \{C_{ikj\ell}(\mathbf{r})\}$ relating stress and strain. We will consider earth models that rotate with a steady angular velocity $\boldsymbol{\Omega}$, aligned with the $\hat{\mathbf{z}}$ axis. The centripetal potential associated with rotation $\psi(\mathbf{r})$ is

$$\psi(\mathbf{r}) = -\tfrac{1}{2}[\Omega^2 r^2 - (\boldsymbol{\Omega} \cdot \mathbf{r})^2] \tag{6}$$

where $\Omega = |\boldsymbol{\Omega}|$, $r = |\mathbf{r}|$. The gravitational potential is related to the density via the Poisson equation

$$\nabla^2 \phi(\mathbf{r}) = 4\pi G \rho(\mathbf{r}) \tag{7}$$

where ∇^2 is the Laplacian operator and G is the gravitational constant. We define the geopotential $\Phi_0(\mathbf{r}) = \phi(\mathbf{r}) + \psi(\mathbf{r})$. The value of apparent "gravity" for which the mass at position $\mathbf{r}$ is at equilibrium on the rotating earth is $-\nabla\Phi_0(\mathbf{r})$. Consider an elastic-gravitational disturbance characterized by a vector displacement function $\mathbf{s}(\mathbf{r})$ and a gravitational potential disturbance $\phi_1(\mathbf{r})$. The linearized equations of motion in the frequency domain that govern this motion are [*Dahlen*, 1973]

$$\rho(-\omega^2 \mathbf{s} + 2i\omega\boldsymbol{\Omega} \times \mathbf{s} + \nabla\phi_1 + \mathbf{s} \cdot \nabla\nabla\Phi_0) = \nabla \cdot \tilde{\mathbf{T}} \tag{8}$$

$$\nabla^2 \phi_1 = 4\pi G \rho_1$$

where

$$\rho_1 = -\nabla \cdot (\rho \mathbf{s}) \tag{9}$$

ω is angular frequency, $i^2 = -1$, and ∇ and $\nabla\nabla$ are the vector gradient and dyadic derivative, respectively. $\tilde{\mathbf{T}}(\mathbf{r})$ is the incremental Piola-Kirchhoff stress tensor related to the incremental strain $\boldsymbol{\epsilon} = \tfrac{1}{2}[\nabla\mathbf{s} + (\nabla\mathbf{s})^T]$ by

$$\tilde{\mathbf{T}} = \boldsymbol{\Lambda} : \boldsymbol{\epsilon} \tag{10}$$

This double-dot product represents

$$\tilde{T}_{ij} = \Lambda_{ijk\ell}\, \epsilon_{k\ell} \tag{11}$$

using the standard index summation convention. The fourth-order tensor $\{\Lambda_{ijk\ell}\}$ may be expressed in terms of the elastic tensor $\{C_{ijk\ell}\}$ and the initial stress field $\mathbf{T}_0$.

$$\Lambda_{ijk\ell} = C_{ijk\ell} + \tfrac{1}{2}(T^0_{ij}\delta_{k\ell} + T^0_{k\ell}\delta_{ij} + T_{ik}\delta_{j\ell} - T^0_{jk}\delta_{i\ell} - T^0_{i\ell}\delta_{jk} - T^0_{j\ell}\delta_{ik}) \tag{12}$$

There exist solutions of (8) at a denumerably infinite number of eigenfrequencies ω_k. On a nonrotating spherical earth model the equations of motion can be solved in terms of vector spherical harmonics. One expresses $\mathbf{s}(\mathbf{r}) = \mathbf{s}(r,\theta,\phi)$

$$\mathbf{s} = {}_nU_\ell(r)\hat{\mathbf{r}}\, Y^m_\ell(\theta,\phi) + {}_nV_\ell(r)\nabla_1 Y^m_\ell(\theta,\phi) - {}_nW_\ell(r)\hat{\mathbf{r}} \times \nabla_1 Y^m_\ell(\theta,\phi) \tag{13}$$

where $\hat{\mathbf{r}}, \hat{\boldsymbol{\theta}}, \hat{\boldsymbol{\phi}}$ are unit vectors in the spherical coordinate directions, $\nabla_1 = \hat{\boldsymbol{\theta}}\partial_\theta + \text{cosec}\theta\hat{\boldsymbol{\phi}}\partial_\phi$ is the spherical surface gradient, and $Y^m_\ell(\theta,\phi)$ are scalar spherical harmonics of angular degree ℓ and azimuthal order m. The subscript n refers to overtone number. We use the definition of *Edmonds* [1960], in which the spherical harmonics are normalized by

$$\int_0^{2\pi}\int_0^{\pi} [Y^{m'}_{\ell'}(\theta,\phi)]^* Y^m_\ell(\theta,\phi)\sin\theta\, d\theta\, d\phi = \delta_{mm'}\delta_{\ell\ell'} \tag{14}$$

where integration is over the unit sphere. We use complex-valued harmonics to represent more easily rotational splitting and coupling. On a spherical nonrotating

earth model, each overtone number/angular degree pair (n,l) defines a multiplet within which the $2l+1$ azimuthal orders $-l \leqslant m \leqslant l$ of the lth degree spherical harmonic label individual singlets. Each singlet represents a possible angular pattern of motion at the degenerate multiplet frequency ${}_n\omega_l$.

A variational principle can be obtained from (8) by taking its scalar product with $D_t\mathbf{s}^*$, where D_t is the substantial (Lagrangian) time derivative and $\mathbf{s}^*$ is the complex conjugate of $\mathbf{s}$. One integrates the resulting scalar quantity over the earth's volume V to obtain an expression for the Lagrangian of the system governed by Hamilton's variational principle. *Woodhouse and Dahlen* [1978] give the desired expressions in terms of an integral functional $L(\omega,\mathbf{s},\phi_1)$ given by

$$L = \int_V \tilde{\mathrm{L}}(\mathbf{s}^*,\phi^*,\mathbf{s},\phi_1)dV + \int_\Sigma [\tilde{\mathrm{M}}(\mathbf{s}^*,\phi^*,\mathbf{s},\phi)]^+_- d\Sigma \quad (15)$$

where

$$\tilde{\mathrm{L}} = \rho(-\omega^2\mathbf{s}^*\cdot\mathbf{s} + 2i\omega\mathbf{s}^*\cdot(\boldsymbol{\Omega}\times\mathbf{s}) + \mathbf{s}^*\cdot\nabla\phi_1 + \mathbf{s}\cdot\nabla\phi_1^* + \mathbf{s}^* \cdot\nabla\nabla\Phi\cdot\mathbf{s}) + (4\pi G)^{-1}|\nabla\phi_1|^2 + \boldsymbol{\epsilon}:\boldsymbol{\Lambda}:\boldsymbol{\epsilon} \quad (16)$$

and

$$\tilde{\mathrm{M}} = \tfrac{1}{2}[(\hat{\mathbf{n}}\cdot\mathbf{s}^*)\nabla_\Sigma\cdot(\pi_0\mathbf{s}) + (\hat{\mathbf{n}}\cdot\mathbf{s})\nabla_\Sigma\cdot(\pi_0\mathbf{s}^*) - \pi_0\mathbf{s}^* \cdot(\nabla_\Sigma\mathbf{s})\cdot\hat{\mathbf{n}} - \pi_0\mathbf{s}\cdot(\nabla_\Sigma\mathbf{s}^*)\cdot\hat{\mathbf{n}}] \quad (17)$$

The surface integral arises from the extra prestress terms necessary at frictionless internal boundaries. $[\tilde{\mathrm{M}}]^+_-$ vanishes at welded boundaries and at the free surface, contributing to L only at fluid-solid boundaries. The variational principle is satisfied for an elastic-gravitational deformation field $(\mathbf{s},\phi_1)$ at a frequency ω if the functional L is stationary with respect to small perturbations in $\mathbf{s}$ and ϕ_1. Such deformation fields satisfy the equation of motion (8). At solutions of (8) the functional L will vanish as well. As defined, the functionals $\tilde{\mathrm{L}}$ and $\tilde{\mathrm{M}}$ are symmetric in $(\mathbf{s},\phi_1)$ and $(\mathbf{s}^*,\phi_1^*)$. They are therefore Hermitian bilinear forms. It is convenient to rearrange (15)–(17) by powers of ω:

$$L = V(\mathbf{s}^*,\mathbf{s}) + \omega W(\mathbf{s}^*,\mathbf{s}) - \omega^2 T(\mathbf{s}^*,\mathbf{s}) \quad (18)$$

where we have left implicit the dependence on ϕ_1 in the notation of the functionals.

$$T(\mathbf{s}^*,\mathbf{s}) = \int_V \rho\mathbf{s}^*\cdot\mathbf{s}\,dV \quad (19)$$

$$W(\mathbf{s}^*,\mathbf{s}) = \int_V 2i\rho\mathbf{s}^*\cdot(\boldsymbol{\Omega}\times\mathbf{s})dV \quad (20)$$

$$V(\mathbf{s}^*,\mathbf{s}) = \int_V [\rho(\mathbf{s}^*\cdot\nabla\phi_1 + \mathbf{s}\cdot\nabla\phi_1^* + \mathbf{s}^*\cdot\nabla\nabla\Phi\cdot\mathbf{s}) + \frac{1}{4\pi G}|\nabla\phi_1|^2 + \boldsymbol{\epsilon}:\boldsymbol{\Lambda}:\boldsymbol{\epsilon}]dV + \int_\Sigma [\tilde{\mathrm{M}}(\mathbf{s}^*,\mathbf{s})]^+_- d\Sigma \quad (21)$$

are the kinetic energy functional, Coriolis functional, and potential energy functional, respectively. Each of these functionals is Hermitian bilinear in $\mathbf{s}$ and $\mathbf{s}^*$. The functionals V, W, and T are Fourier-transformed quantities that represent time-averaged energy. The variational principle thus formulated becomes

$$L = 0 = V(\mathbf{s}^*,\mathbf{s}) + \omega W(\mathbf{s}^*,\mathbf{s}) - \omega^2 T(\mathbf{s}^*,\mathbf{s}) \quad (22)$$

and

$$\delta L = 0 \quad (23)$$

with respect to small perturbations in $\mathbf{s}$ and ϕ_1.

The numerical application of the variational principle is explicated in many textbooks [*Moiseiwitsch*, 1966; *Marchuk*, 1975]. In the normal mode problem, one selects a basis set of functions $\{\mathbf{s}_1,\mathbf{s}_2,\cdots,\mathbf{s}_N\}$, where we have again left the gravitational perturbation implicit. These basis functions have sufficient smoothness for the differential equation and also satisfy the unperturbed boundary conditions. One constructs an eigenfunction-eigenfrequency pair with a linear combination of the $\mathbf{s}_i$. Let $\mathbf{s} = \alpha_i\mathbf{s}_i$, with sum over i implicit. Substitution into (22) gives

$$0 = L = V(\alpha_i^*\mathbf{s}_i^*,\alpha_j\mathbf{s}_j) + \omega W(\alpha_i^*\mathbf{s}_i^*,\alpha_j\mathbf{s}_j) - \omega^2 T(\alpha_i^*\mathbf{s}_i^*,\alpha_j\mathbf{s}_j) = \alpha_i^*(V_{ij}+\omega W_{ij}-\omega^2 T_{ij})\alpha_j \quad (24)$$

where

$$\begin{aligned} V_{ij} &= V(\mathbf{s}_i^*,\mathbf{s}_j) \\ W_{ij} &= W(\mathbf{s}_i^*,\mathbf{s}_j) \\ T_{ij} &= T(\mathbf{s}_i^*,\mathbf{s}_j) \end{aligned} \quad (25)$$

are the matrix elements of interaction between the basis functions. If we define the N vector $\boldsymbol{\alpha} = (\alpha_1,\cdots,\alpha_N)$, and the interaction matrices $\mathbf{V} = \{V_{ij}\}$, etc., (24) reduces to

$$0 = \boldsymbol{\alpha}^*\cdot(\mathbf{V}+\omega\mathbf{W}-\omega^2\mathbf{T})\cdot\boldsymbol{\alpha} \quad (26)$$

Application of the variational principle gives us a quadratic problem in angular frequency ω. The quantity on the right side of (26) is stationary to small changes in $\boldsymbol{\alpha}$ if and only if $\boldsymbol{\alpha}$ is an eigenvector of $\mathbf{V}+\omega\mathbf{W}-\omega^2\mathbf{T}$. The matrices $\mathbf{V}$, $\mathbf{W}$, and $\mathbf{T}$ are all Hermitian, e.g., $V_{ij} = V_{ji}^*$, as they are projections of Hermitian forms. The quadratic system can be transformed into a linear eigenvalue problem at the expense of doubling the matrix size [*Garbow et al.*, 1977]. Define

$$\tilde{\mathbf{V}} = \begin{bmatrix} \mathbf{W} & \mathbf{V} \\ \mathbf{I} & 0 \end{bmatrix} \qquad \tilde{\mathbf{T}} = \begin{bmatrix} \mathbf{T} & 0 \\ 0 & \mathbf{I} \end{bmatrix} \quad (27)$$

where $\mathbf{I}$ is the $N\times N$ identity matrix. Equation (26) becomes

$$\boldsymbol{\gamma}^*\cdot(\tilde{\mathbf{V}}-\omega\tilde{\mathbf{T}})\cdot\boldsymbol{\gamma} = 0 \quad (28)$$

where

$$\boldsymbol{\gamma} = \begin{bmatrix} \omega\boldsymbol{\alpha} \\ \boldsymbol{\alpha} \end{bmatrix} \quad (29)$$

The eigenvalue problem defined by (28) has $2N$ eigenvalues, whereas we only have N basis vectors. Since the choice of matrix manipulation scheme cannot alter the number of degrees of freedom in the problem, the eigenvalues of (28) must be related. *Dahlen and Smith* [1974] note that if the eigenfunction-eigenfrequency pair $(\mathbf{s},\omega)$ satisfies (22) and (23), then so does $(\mathbf{s}^*,-\omega)$. One forms a sum of the two solutions

$$\begin{aligned} c\mathbf{s}(\mathbf{r})e^{i\omega t} &+ c^*\mathbf{s}^*(\mathbf{r})e^{-i\omega t} \\ c\phi_1(\mathbf{r})e^{i\omega t} &+ c^*\phi_1^*(\mathbf{r})e^{-i\omega t} \end{aligned} \quad (30)$$

where c is an arbitrary complex scalar, to form a real-amplitude standing wave pattern within the earth. Care must be taken in the variational scheme that, if the basis set $\{\mathbf{s}_1 \cdots \mathbf{s}_N\}$ generates an eigenvector $\mathbf{s}'$, the complex conjugate $(\mathbf{s}')^*$ is within the span of $\{\mathbf{s}_1 \cdots \mathbf{s}_N\}$ as well. In practice, this is achieved by either choosing the basis functions $\mathbf{s}_i$ to be purely real, or, for complex-valued vector spherical harmonic expansions, including both its positive and negative azimuthal orders $(\pm m)$. A basis set composed in either manner will yield N eigenvalue pairs $(\omega,-\omega)$ and N pairs of eigenvectors $(\boldsymbol{\gamma}^+,\boldsymbol{\gamma}^-)$. These eigenvectors are related to the solutions of (26) by

$$\boldsymbol{\gamma}^+ = \begin{bmatrix} \omega\boldsymbol{\alpha}^+ \\ \boldsymbol{\alpha}^+ \end{bmatrix} \quad \boldsymbol{\gamma}^- = \begin{bmatrix} -\omega\boldsymbol{\alpha}^- \\ \boldsymbol{\alpha}^- \end{bmatrix} \tag{31}$$

$\boldsymbol{\alpha}^+$ and $\boldsymbol{\alpha}^-$ specify the linear combinations of the basis set $\{\mathbf{s}_1 \cdots \mathbf{s}_N\}$ that combine according to (30) to produce real-amplitude motion.

In the eigensystem in (28), $\tilde{\mathbf{V}}$ is not Hermitian. However, we can perform a similarity transform that will make it so, as long as $\mathbf{V}$ is positive definite as well as Hermitian. Under these conditions, we can form the complex Cholesky decomposition

$$\mathbf{V} = \mathbf{L} \cdot \mathbf{L}^H \tag{32}$$

where $\mathbf{L}$ is a lower triangular complex matrix and $\mathbf{L}^H$ is the Hermitian transpose of $\mathbf{L}$. If we define

$$\tilde{\mathbf{S}} = \begin{bmatrix} \mathbf{I} & 0 \\ 0 & \mathbf{L}^H \end{bmatrix} \tag{33}$$

then $\tilde{\mathbf{S}} \cdot \tilde{\mathbf{T}} \cdot \tilde{\mathbf{S}}^{-1} = \tilde{\mathbf{T}}$ leaves the kinetic energy matrix unchanged and

$$\tilde{\mathbf{S}} \cdot \tilde{\mathbf{V}} \cdot \tilde{\mathbf{S}}^{-1} = \begin{bmatrix} \mathbf{W} & \mathbf{L} \\ \mathbf{L}^H & 0 \end{bmatrix} \tag{34}$$

is Hermitian. The similarity transform leaves the eigenvalues of the system unchanged. The eigenvectors $\boldsymbol{\gamma}_k$ are replaced by $\tilde{\mathbf{S}} \cdot \boldsymbol{\gamma} = (\omega\boldsymbol{\alpha}, \mathbf{L}^H \cdot \boldsymbol{\alpha})$.

$\mathbf{V}$ is not positive definite in cases where the degrees of freedom spanned by the basis set $\{\mathbf{s}_1 \cdots \mathbf{s}_N\}$ include either secular motion (e.g., rigid rotation of the mantle about the rotation axis) or unstable motion in the outer core. Many standard earth models have regions in the outer core with imaginary Brunt-Väisälä frequency [*Masters*, 1979]. For these models there exist normal modes with imaginary eigenfrequency. Secular modes have zero frequency, and (28) will yield two eigenvectors

$$\boldsymbol{\gamma}^+ = \begin{bmatrix} 0 \\ \boldsymbol{\alpha}^+ \end{bmatrix} \quad \boldsymbol{\gamma}^- = \begin{bmatrix} 0 \\ \boldsymbol{\alpha}^- \end{bmatrix} \tag{35}$$

If $\boldsymbol{\alpha}^+ = \boldsymbol{\alpha}^-$ the matrix $\tilde{\mathbf{V}}$ is formally defective. The numerically derived eigenvector associated with the defective eigenvalue should be used with caution, if at all. In studies of free oscillation behavior, at all but the lowest frequencies the potential energy matrix $\mathbf{V}$ will be positive definite. *Park* [1985] describes coupling results for the mode ${}_0S_2$ for cases where $\mathbf{V}$ is singular.

Let $S = \{\mathbf{s}_1, \cdots, \mathbf{s}_N\}$ be a set of normal mode eigenfunctions of a nonrotating, elastic isotropic spherical earth model, referred to as the "terrestrial monopole." The "terrestrial monopole" nomenclature also refers to models that possess radially dependent anelasticity and whose attenuative effects on basis set modes are calculated with first-order perturbation theory. S is a global basis, as its members are nonvanishing over the whole of the earth's volume V where that type of mode can be defined, e.g., all of V for spheroidal modes, the mantle and crust for mantle toroidal modes. Let $\{\omega_{o1}, \omega_{o2}, \cdots, \omega_{oN}\}$ be the eigenfrequencies of the basis set S with respect to the terrestrial monopole. Typically, these frequencies are grouped into degenerate multiplet frequencies. Rotation, anisotropy, and lateral structure can be viewed as perturbations to the terrestrial monopole, and their effect can be quantified through Rayleigh's principle. First-order perturbation theory based on Rayleigh's principle has been developed by *Dahlen* [1968, 1969], *Madariaga* [1971], *Zharkov and Lubimov* [1970*a*,*b*], and others. The extension of perturbation theory to a global variational procedure using many different multiplets has been applied by *Luh* [1974], *Stifler and Bolt* [1981], *Morris and Geller* [1982], *Kawakatsu and Geller* [1981], *Tanimoto and Bolt* [1983], and others. The formulation of Rayleigh's principle for perturbations to density ρ, isotropic elastic parameters μ,κ, and boundaries, as well as rotation, deviatoric prestress, and general anisotropy are given by *Woodhouse and Dahlen* [1978]. Expressions for all but the last two effects in a form more suitable for computation are given in the appendix of *Woodhouse* [1980]. Continuous volume perturbations in ρ,κ, and μ involve no approximations to the general variational principle (24) on the finite basis set S. The rotational terms of *Woodhouse and Dahlen* [1978] neglect the second-order interaction of the earth's rotation with its induced equatorial bulge, which is important only for certain secular modes. Terms appropriate to deformations at earth discontinuity surfaces involve an approximation because members of the global basis S fit the boundary conditions on the undeformed boundary. *Woodhouse* [1976] shows how boundary deformations can be handled to first order in Rayleigh's priciple. If the boundary perturbations are small, the spherical earth eigenfunctions should be adequate to model observations of free oscillation data.

We reformulate (24) by taking $V_0(\mathbf{s}^*,\mathbf{s})$, $T_0(\mathbf{s}^*,\mathbf{s})$ and $\delta V(\mathbf{s}^*,\mathbf{s})$, $\delta T(\mathbf{s}^*,\mathbf{s})$ as functionals for the terrestrial monopole and the aspherical component of the given earth model, respectively:

$$\begin{aligned} V(\mathbf{s}^*,\mathbf{s}) &\simeq V_0(\mathbf{s}^*,\mathbf{s}) + \delta V(\mathbf{s}^*,\mathbf{s}) \\ T(\mathbf{s}^*,\mathbf{s}) &\simeq T_0(\mathbf{s}^*,\mathbf{s}) + \delta T(\mathbf{s}^*,\mathbf{s}) \end{aligned} \tag{36}$$

$\delta V(\mathbf{s}^*,\mathbf{s})$ will contain interaction terms due to the centripetal force. If $v_{ij} = \delta V(\mathbf{s}^*,\mathbf{s})$, $t_{ij} = \delta T(\mathbf{s}^*,\mathbf{s})$,

$$\begin{aligned} V_{ij} &= \omega_{oi}^2 \delta_{ij} + v_{ij} \\ T_{ij} &= \delta_{ij} + t_{ij} \end{aligned} \tag{37}$$

where ω_{oi} is the unperturbed frequency of the ith singlet. We have used the normalization convention

$$T_0(\mathbf{s}_i^*,\mathbf{s}_j) = \delta_{ij} \tag{38}$$

For reasonable aspherical models, $t_{ij} << 1$ for all modes of interest, and $v_{ij} << \omega_{oi}\omega_{oj}$ when $\mathbf{s}_i,\mathbf{s}_j$ are not secular motions or outer core gravitational modes. When the

basis set S does not contain any such zero or nearly zero frequency spherical earth modes, both $\mathbf{V}$ and $\mathbf{T}$ are diagonally dominant matrices. Since the earth rotation frequency $\Omega/(2\pi) \cong 11.6\,\mu$Hz satisfies $\Omega << \omega$ for all frequencies of interest in terrestrial seismology, the Coriolis functional matrix element satisfies $\omega w_{ij} << (\omega_{oi}\omega_{oj})$ when $\mathbf{s}_i, \mathbf{s}_j$ are not zero or nearly zero frequency motions of the terrestrial monopole. It is conventional to choose a fiducial frequency $\hat{\omega}_0$ and absorb the matrix $\mathbf{W}$ into the potential energy matrix $\mathbf{V}$ to form a new interaction matrix

$$\tilde{\mathbf{V}} = \mathbf{V} + \hat{\omega}_0 \mathbf{W} \tag{39}$$

The immediate advantage of (39) is that it reduces (26) to a linear eigenvalue problem in ω^2 of order N. We test the numerical validity of (39) in a later section.

We wish to solve the linear eigenvalue problem $(\tilde{\mathbf{V}} - \omega^2 \mathbf{T}) \cdot \boldsymbol{\alpha} = 0$. $\mathbf{T}$ is positive definite Hermitian, so the complex Cholesky decomposition $\mathbf{T} = \mathbf{L} \cdot \mathbf{L}^H$ exists, where $\mathbf{L}$ is a complex lower triangular matrix with inverse $\mathbf{L}^{-1}$. The eigenvalue problem becomes

$$(\mathbf{L}^{-1} \cdot \tilde{\mathbf{V}} \cdot \mathbf{L}^{-H} - \omega^2 \mathbf{I}) \cdot (\mathbf{L}^H \cdot \boldsymbol{\alpha}) = (\tilde{\mathbf{V}}' - \omega^2 \mathbf{I}) \cdot \tilde{\boldsymbol{\alpha}} = 0 \tag{40}$$

We can decompose $\tilde{\mathbf{V}}'$ into its eigenvalues and eigenvectors

$$\tilde{\mathbf{V}}' = \mathbf{U} \cdot \mathbf{D} \cdot \mathbf{U}^H \tag{41}$$

where $\mathbf{D} = \text{diag}\{\omega_1^2, \omega_2^2, \cdots, \omega_N^2\}$ contains the squared hybrid eigenfrequencies ω_k^2 and the columns of $\mathbf{U}$ contain the eigenvectors $\tilde{\boldsymbol{\alpha}}_k$ of $\tilde{\mathbf{V}}'$. The $\tilde{\boldsymbol{\alpha}}_k$ are orthonormal with respect to the complex inner product $\tilde{\boldsymbol{\alpha}}_i^* \cdot \tilde{\boldsymbol{\alpha}}_j = \delta_{ij}$, and the ω_k^2 are real. A further transformation $\boldsymbol{\alpha}_k = \mathbf{L}^{-H} \cdot \tilde{\boldsymbol{\alpha}}_k$ obtains the linear combinations of spherical earth singlets that comprise the desired hybrid normal mode free oscillation singlets. The $\boldsymbol{\alpha}_i$ satisfy the orthogonality condition

$$\boldsymbol{\alpha}_i^* \cdot \mathbf{T} \cdot \boldsymbol{\alpha}_j = \tilde{\boldsymbol{\alpha}}_i^* \cdot \mathbf{L}^{-1} \cdot \mathbf{T} \cdot \mathbf{L}^{-H} \cdot \tilde{\boldsymbol{\alpha}}_j^* = \delta_{ij} \tag{42}$$

Since $\mathbf{T}$ is close to the identity matrix ($t_{ij} \lesssim$ the maximum fractional change in density, presumably small except in the crust), the $\boldsymbol{\alpha}_k$ are nearly orthonormal.

The solution to the quadratic eigenvalue problem is similar. If $\mathbf{T} = \mathbf{L} \cdot \mathbf{L}^H$, $\mathbf{V}' = \mathbf{L}^{-1} \cdot \mathbf{V} \cdot \mathbf{L}^{-H}$, $\mathbf{W}' = \mathbf{L}^{-1} \cdot \mathbf{W} \cdot \mathbf{L}^{-H}$, and

$$\tilde{\mathbf{V}}' = \begin{bmatrix} \mathbf{W}' & \mathbf{V}' \\ \mathbf{I} & 0 \end{bmatrix} \tag{43}$$

then solution of the linear eigenvalue problem $(\tilde{\mathbf{V}}' - \omega \tilde{\mathbf{I}}) \cdot \tilde{\boldsymbol{\gamma}} = 0$, where $\tilde{\mathbf{I}}$ is the $2N \times 2N$ identity matrix, will yield hybrid eigenfrequencies $\pm\omega_k$ and eigenvectors $\tilde{\boldsymbol{\gamma}}_k^{\pm}$ such that

$$\tilde{\boldsymbol{\gamma}}_k^{\pm} = \begin{bmatrix} \pm\omega_k \tilde{\boldsymbol{\alpha}}_k^{\pm} \\ \tilde{\boldsymbol{\alpha}}_k^{\pm} \end{bmatrix} \tag{44}$$

The desired hybrid singlets are again obtained by the formula $\boldsymbol{\alpha}_k^{\pm} = \mathbf{L}^{-H} \tilde{\boldsymbol{\alpha}}_k^{\pm}$. Only the $\boldsymbol{\alpha}_k^+$ are needed in the calculation of synthetic seismograms.

The excitation of seismic motion by an earthquake source can be expressed for both rotating and nonrotating earth models. *Dahlen* [1978] shows that the two cases differ by a term proportional to $\delta\Omega/\Omega$, the fractional change in the earth's rotation frequency caused by the redistribution of mass following an earthquake. This term arises from coupling of the elastic-gravitational normal modes with the secular axial spin modes of the earth. For almost all seismic applications, the excitation expansion for the nonrotating case is adequate. If the seismic source is modeled as a point source, it can be defined by a frequency-dependent moment tensor $\mathbf{M}(\omega)$. For an earthquake that occurs at point $\mathbf{r}_o$ the particle motion $\mathbf{u}$ at point $\mathbf{r}$ as a function of frequency can be expressed [*Gilbert and Dziewonski*, 1975] as

$$\mathbf{u}(\mathbf{r},\omega) = \sum_k \tilde{\mathbf{s}}_k(\mathbf{r})[\mathbf{M}(\omega) : \boldsymbol{\epsilon}_k^*(\mathbf{r}_o)] C_k(\omega) \tag{45}$$

where $\boldsymbol{\epsilon}_k^*(\mathbf{r}_o) = \frac{1}{2}\{\nabla \tilde{\mathbf{s}}_k^*(\mathbf{r}_o) + [\nabla \tilde{\mathbf{s}}_k^*(\mathbf{r}_o)]^T\}$ is the complex conjugated strain at the source position $\mathbf{r}_o$ associated with the hybrid free oscillation singlet $\tilde{\mathbf{s}}_k$. $C_k(\omega)$ is the singlet resonance function, well approximated by $\omega_k^{-2} i(\omega - \omega_k)^{-1}$ on a nondissipative earth. The sum extends over all normal modes. $C_k(\omega)$ differs from the Gilbert and Dziewonski expression by a factor of ω_k^2, as we have adopted a different normalization condition, and by the absence of a dissipation parameter α_k.

We restrict attention to a narrow band of frequency $\omega_c \pm \Delta\omega$ containing N spherical earth singlets $\mathbf{s}_j$. The rotating, aspherical earth singlets $\tilde{\mathbf{s}}_k$ within this band can be approximated by hybrid combinations

$$\tilde{\mathbf{s}}_k = \sum_{j=1}^{N} \alpha_{kj} \mathbf{s}_j$$

Let $\boldsymbol{\epsilon}_j = \frac{1}{2}[\nabla \mathbf{s}_j + (\nabla \mathbf{s}_j)^T]$ be the strain associated with the spherical earth singlet $\mathbf{s}_j$. Equation (45) becomes, over the bandwidth $\omega_c \pm \Delta\omega$,

$$\mathbf{u}(\mathbf{r},\omega) = \sum_{i=1}^{N} \sum_{j=1}^{N} \sum_{k=1}^{N} \alpha_{ki} \alpha_{kj}^* \mathbf{s}_i(\mathbf{r})[\mathbf{M}(\omega) : \boldsymbol{\epsilon}_j^*(\mathbf{r}_o)] C_k(\omega) \tag{46}$$

The contribution from the resonance peaks outside $\omega_c \pm \Delta\omega$ is neglected. Equation (46) shows how excitation calculations for a spherical earth model can be extended to aspherical models.

4. GALERKIN THEORY: DISSIPATIVE EARTH MODELS

The recipe for the Galerkin procedure parallels that for the variational principle. Let the set of functions $\{\mathbf{s}_1, \mathbf{s}_2, \cdots, \mathbf{s}_N\}$ be a set of normal mode eigenfunctions for a terrestrial monopole. We decompose the kinetic and potential energy functions as in (36) into terms $V_0(\mathbf{s}^*, \mathbf{s})$, $T_0(\mathbf{s}^*, \mathbf{s})$ representing the terrestrial monopole and $\delta V(\mathbf{s}^*, \mathbf{s})$, $\delta T(\mathbf{s}^*, \mathbf{s})$ representing a given model for asphericity and attenuation. The need to model physical dispersion in tandem with attenuation was first pointed out by *Akopyan et al.* [1975, 1976]. We model attenuation by assuming the absorption band model put forward by *Liu et al.* [1976]. The elastic moduli μ and κ become complex and frequency dependent according to the relations

$$\begin{aligned} \mu(\mathbf{r},\omega) &= \mu_0(r)\{1 + Q_\mu^{-1}(r)[(2/\pi)\ln(\omega/\hat{\omega}_0) - i]\} + \delta\mu(\mathbf{r}) \\ \kappa(\mathbf{r},\omega) &= \kappa_0(r)\{1 + Q_\kappa^{-1}(r)[(2/\pi)\ln(\omega/\hat{\omega}_0) - i]\} + \delta\kappa(\mathbf{r}) \end{aligned} \tag{47}$$

$\delta\mu, \delta\kappa$ are the aspherical perturbations to the terrestrial

monopole elastic parameters μ_0, κ_0. Q_μ, Q_κ are spherically averaged quality factors that vary with radius but not with frequency within a specified absorption band. This band is typically taken to cover all measured free oscillation frequencies. The $\hat{\omega}_0$ is a reference frequency for the logarithmic dispersive term. Seismic evidence for lateral variations in mantle Q structure has been cited for ScS body wave phases by *Sipkin and Jordan* [1980]. There is as yet no persuasive evidence in low-frequency seismology for such heterogeneity. *Masters and Gilbert* [1983] found that Q estimates measured from fundamental spheroidal mode ${}_0S_\ell$ resonance peaks varied widely among records. However, this variation showed no robust pattern with source-receiver orientation and was taken to be caused by the interference effects of lateral structure. This conclusion is supported by *Park* [1985] and *Davis* [1985] where a similar variability was found in Q estimates made from synthetic seismograms obtained from the lateral structure model of *Woodhouse and Dziewonski* [1984], which has no lateral variation in attenuation. For this reason we have chosen not to model lateral variation in Q-structure in our calculations. The interaction matrix will therefore have a small imaginary part on the diagonal, causing the matrix system to be complex. It is useful to separate the interactions due to dispersion to obtain a new functional expression

$$L = V(\mathbf{s}^*,\mathbf{s}) + \ln(\omega/\hat{\omega}_0)\, V_D(\mathbf{s}^*,\mathbf{s}) + \omega\, W(\mathbf{s}^*,\mathbf{s}) - \omega^2 T(\mathbf{s}^*,\mathbf{s}) \tag{48}$$

where the dispersive interactions are included in the functional $V_D(\mathbf{s}^*,\mathbf{s})$. We seek $\omega,\mathbf{s}$ for which L is stationary. Since the absorption band dissipation model is not intended for modes at zero frequency, the logarithmic term causes formal problems if secular modes are considered. We restrict attention to seismic modes. For computational purposes we replace $\ln(\omega/\hat{\omega}_0)$ by its Taylor series. Let $\eta = (\omega-\hat{\omega}_0)/\hat{\omega}_0$. Then

$$\ln(\omega/\hat{\omega}_0) = \ln(1+\eta) = \eta - \frac{\eta^2}{2} + \frac{\eta^3}{3} - \frac{\eta^4}{4} + \cdots \tag{49}$$

If $\omega_0 = 3$ mHz and $|\omega-\omega_0| \leqslant 0.2$ mHz, $\eta \leqslant 0.067$ and we can truncate (49) at the quadratic term with a relative error $\leqslant 0.005$ in this case. We adopt this truncation in general to avoid higher-order eigenproblems. The new relation becomes

$$L = V(\mathbf{s}^*,\mathbf{s}) - \frac{\omega^2 - 4\omega\hat{\omega}_0 + 3\hat{\omega}_0^2}{2\hat{\omega}_0^2}\, V_D(\mathbf{s}^*,\mathbf{s}) + \omega\, W(\mathbf{s}^*,\mathbf{s}) - \omega^2 T(\mathbf{s}^*,\mathbf{s}) \tag{50}$$

Note that the dispersion term has a component linear in ω.

We seek linear combinations of spherical earth eigenfunctions with zeroth-order eigenfrequencies near the fiducial frequency $\hat{\omega}_0$ that make (50) stationary. As in the variational problem, the hybrid eigenfunction is a linear combination of basis set functions $\mathbf{s} = \alpha_i \mathbf{s}_i$. We allow for the lack of symmetry in the attenuative-dispersive operator by seeking an adjoint solution $\tilde{\mathbf{s}} = \beta_i \mathbf{s}_i^*$. With no attenuation $\beta_i = \alpha_i^*$. The Galerkin procedure on this basis set is equivalent to the eigenvalue problem

$$O = L = \boldsymbol{\beta} \cdot [\mathbf{V} - \tfrac{3}{2}\mathbf{V}_D + \omega(\mathbf{W} + 2\hat{\omega}_0^{-1}\mathbf{V}_D) - \omega^2(\mathbf{T} + \tfrac{1}{2}\hat{\omega}_0^{-2}\mathbf{V}_D)] \cdot \boldsymbol{\alpha} \tag{51}$$

where

$$(\mathbf{V}_D)_{ij} = V_D(\mathbf{s}_i^*,\mathbf{s}_j) \tag{52}$$

The right and left eigenvectors $\boldsymbol{\alpha}_k, \boldsymbol{\beta}_k$ of (51) represent the eigenfunctions and adjoint eigenfunctions of the attenuative-dispersive free oscillation operator projected onto the basis set $\{\mathbf{s}_1 \cdots \mathbf{s}_N\}$. For computational convenience we normalize these vectors by the rule

$$\boldsymbol{\beta}_i \cdot (\mathbf{T} + \tfrac{1}{2}\hat{\omega}_0^{-2}\mathbf{V}_D) \cdot \boldsymbol{\alpha}_j = \delta_{ij} \tag{53}$$

To solve (51), decompose

$$\mathbf{T} + \tfrac{1}{2}\omega_0^{-2}\mathbf{V}_D = \mathbf{L} \cdot \mathbf{L}^H \tag{54}$$

This decomposition is valid since $\mathbf{T}$ and $\mathbf{V}_D$ are both Hermitian. We form $\mathbf{V}' = \mathbf{L}^{-1} \cdot (\mathbf{V} - \frac{3}{2}\mathbf{V}_D) \cdot \mathbf{L}^{-H}$ and $\mathbf{W}' = \mathbf{L}^{-1} \cdot (\mathbf{W} + 2\hat{\omega}_0^{-1}\mathbf{V}_D) \cdot \mathbf{L}^{-H}$ in order to construct

$$\tilde{\mathbf{V}}' = \begin{bmatrix} \mathbf{W}' & \mathbf{V}' \\ \mathbf{I} & 0 \end{bmatrix} \tag{55}$$

As in the variational case, we must solve the linear eigenvalue problem $(\tilde{\mathbf{V}}' - \omega\tilde{\mathbf{I}}) \cdot \tilde{\boldsymbol{\gamma}} = 0$ to obtain hybrid eigenfrequencies and eigenvectors.

If the linear term in ω is not desired, we take $\omega = \hat{\omega}_0$ as before to form the generalized eigenvalue problem

$$\{\mathbf{V} + (\tfrac{1}{2})\mathbf{V}_D + \hat{\omega}_0\mathbf{W} - \omega^2[\mathbf{T} + (\tfrac{1}{2})(\hat{\omega}_0)^{-2}\mathbf{V}_D]\} \cdot \boldsymbol{\alpha} = 0 \tag{56}$$

Taking $\tilde{\mathbf{V}}' = \mathbf{L}^{-1} \cdot [\mathbf{V} + (\tfrac{1}{2})\mathbf{V}_D + \hat{\omega}_0\mathbf{W}] \cdot \mathbf{L}^{-H}$, we have the counterpart of (40)

$$(\tilde{\mathbf{V}}' - \omega^2\mathbf{I}) \cdot (\mathbf{L}^H \cdot \boldsymbol{\alpha}) = (\tilde{\mathbf{V}}' - \omega^2\mathbf{I}) \cdot \tilde{\boldsymbol{\alpha}} = 0 \tag{57}$$

We restrict the following discussion to the solution of (57), as the generalization to the quadratic eigenvalue problem has been discussed in the previous section.

Although the effect of physical dispersion is self-adjoint in character, the effect of finite dissipation is not. If $\kappa(r,\omega)$ and $\mu(r,\omega)$ are modeled as in (47), the diagonal terms of the potential energy matrix $\mathbf{V}$ will gain a small imaginary part. $\mathbf{V}$ is no longer Hermitian. If two distinct singlets with the same angular dependence (e.g., ${}_{10}S_2^2$ and ${}_{11}S_2^2$) are included in the Galerkin basis set $\{\mathbf{s}_1 \cdots \mathbf{s}_N\}$, there will be a small off-diagonal non-Hermitian part as well. $\tilde{\mathbf{V}}'$ is a general complex matrix, as multiplication by the Cholesky factors spreads the non-Hermitian part off the diagonal. Thus the Galerkin procedure easily includes aspherical attenuation. The decomposition of $\tilde{\mathbf{V}}'$ differs from (41) in a potentially drastic manner. $\tilde{\mathbf{V}}'$ has both right-eigenvectors $\tilde{\boldsymbol{\alpha}}_k$ and left- (or adjoint) eigenvectors $\tilde{\boldsymbol{\beta}}_k$. If $\omega_i \neq \omega_j$, $\tilde{\boldsymbol{\alpha}}_i \cdot \tilde{\boldsymbol{\beta}}_j = \tilde{\boldsymbol{\beta}}_i \cdot \tilde{\boldsymbol{\alpha}}_j = 0$, but $\tilde{\boldsymbol{\alpha}}_i \cdot \tilde{\boldsymbol{\alpha}}_j \neq 0$ and $\tilde{\boldsymbol{\beta}}_i \cdot \tilde{\boldsymbol{\beta}}_j \neq 0$. If an eigenfrequency ω_i is k-fold degenerate, we are not guaranteed k linearly independent right-eigenvectors for ω_i. The same is true for left-eigenvectors. A $N \times N$ matrix with fewer than N linearly independent right- (or left-) eigenvectors is called defective. A truly defective free oscillation interaction matrix would be unlikely, as only accidental frequency degeneracy can occur on a rotating earth. Unfortunately there are many cases of near-degeneracy, some of which give rise to

nearly defective attenuative-dispersive interaction matrices.

If $\tilde{\mathbf{V}}'$ is not defective, it can be decomposed as

$$\mathbf{V}' = \mathbf{S} \cdot \mathbf{D} \cdot \mathbf{S}^{-1} \tag{58}$$

where $\mathbf{S}$ is a nonsingular matrix and $\mathbf{D}$ is a diagonal matrix of squared hybrid frequencies ω_i. The columns of $\mathbf{S}$ are the right-eigenvectors $\tilde{\boldsymbol{\alpha}}_i$ of $\tilde{\mathbf{V}}'$. The rows of $\mathbf{S}^{-1}$ are the left-eigenvectors $\tilde{\boldsymbol{\beta}}_i$. If $\tilde{\mathbf{V}}'$ were Hermitian, $\mathbf{S}$ would be unitary as in (41) and, since $\mathbf{S}^{-1} = \mathbf{S}^H$ for unitary $\mathbf{S}$, $\tilde{\boldsymbol{\beta}}_i$ would equal $\tilde{\boldsymbol{\alpha}}_i^*$. $\tilde{\mathbf{V}}'$ is "similar" to the diagonal matrix $\mathbf{D}$ according to (58). Mathematically speaking, this relation is much less symmetric than "unitary similarity" as expressed in the decomposition (41). Although the right and left eigenvectors $\tilde{\boldsymbol{\alpha}}_k$ and $\tilde{\boldsymbol{\beta}}_k$ are "dual" (i.e., $\tilde{\boldsymbol{\alpha}}_k \cdot \tilde{\boldsymbol{\beta}}_j = \delta_{kj}$), pairs of the $\tilde{\boldsymbol{\alpha}}_k$ (alternatively pairs of $\tilde{\beta}_k$) can be nearly parallel in N space. As in the Hermitian case we transform with the Cholesky factors of $\mathbf{T}$ to obtain eigenvectors appropriate to our perturbed earth model

$$\begin{aligned} \boldsymbol{\alpha}_k &= \mathbf{L}^{-H} \cdot \tilde{\boldsymbol{\alpha}}_k \\ \boldsymbol{\beta}_k &= \tilde{\boldsymbol{\beta}}_k \cdot \mathbf{L}^{-1} \\ \boldsymbol{\alpha}_k \cdot \boldsymbol{\beta}_\ell &= (\mathbf{T}^{-1})_{k\ell} \end{aligned} \tag{59}$$

Since $\mathbf{T}$ differs only slightly from the identity, $\{\boldsymbol{\alpha}_1 \cdots \boldsymbol{\alpha}_N\}$ and $\{\boldsymbol{\beta}_1 \cdots \boldsymbol{\beta}_N\}$ are nearly dual to each other.

Both eigenvector sets are necessary to construct a synthetic seismogram. As before, we restrict attention to a set of N spherical earth singlets $\mathbf{s}_j$ that are nearby in frequency. The hybrid singlets, as in the Hermitian case, are

$$\tilde{\mathbf{s}}_k = \sum_{j=1}^{N} \alpha_{kj} \mathbf{s}_j$$

where α_{kj} is the jth component of $\boldsymbol{\alpha}_k$. We define adjoint hybrid singlets

$$\bar{\tilde{\mathbf{s}}}_k = \sum_{j=1}^{N} \beta_{kj} \mathbf{s}_j^*$$

where β_{kj} is the jth component of $\boldsymbol{\beta}_k$. When we apply the formula for seismic particle motion (45), we must express $\boldsymbol{\epsilon}_k^*(r_o)$ in terms of the adjoint hybrid singlets $\bar{\tilde{\mathbf{s}}}_k$. The particle motion $\mathbf{u}(\mathbf{r},\omega)$ at frequency ω and position $\mathbf{r}$ due to these singlets is, analogous to (46)

$$\mathbf{u}(\mathbf{r},\omega) = \sum_{i=1}^{N} \sum_{j=1}^{N} \sum_{k=1}^{N} \alpha_{ki} \beta_{kj} \mathbf{s}_i(\mathbf{r}) [\mathbf{M}(\omega) : \boldsymbol{\epsilon}_j^*(\mathbf{r}_o)] C_k(\omega) \tag{60}$$

The definitions of $\mathbf{M}(\omega)$, $\boldsymbol{\epsilon}_j^*$, $\mathbf{r}_o$ and C_k are unchanged from those of (46).

The Galerkin formalism is more complicated than the variational formalism, the latter being a special case of the former. The additional flexibility afforded by the Galerkin formalism is crucial to many coupling problems where the effect of attenuation can be very important.

5. NUMERICAL TESTS OF GALERKIN PROCEDURE: QUADRATIC EFFECTS

The Galerkin principle can be applied to the free oscillations of a rotating general earth model in either a linear or quadratic eigenvalue-eigenvector scheme. The quadratic scheme is a more accurate representation of the physical problem, but its application doubles the size of the eigenvalue problem to be solved. This increases the amount of computation required by a factor of 8, as an eigenvalue problem of order N requires kN^3 operations. The k is a constant of order 1—10 that depends on the type of matrix and the matrix algorithm chosen. On computers with vector processing hardware the CPU time required can be made to vary as N^2. Even with this improvement the extra precision is bought dearly. It is important to assess where the quadratic effects are important and where they can be ignored. We will compare quadratic and linear perturbation formulae for a rotating elliptical earth and numerical examples for an earth model with the transition zone anomaly of *Masters et al.* [1982].

First-order perturbation theory for rotation and ellipticity [*Dahlen*, 1968] results in a singlet frequency splitting pattern that is quadratic in azimuthal order m

$${}_n\omega_\ell^m = {}_n\omega_\ell (1 + a + bm + cm^2) \tag{61}$$

where ${}_n\omega_\ell$ is the degenerate multiplet frequency and a, b, c are splitting parameters that depend on the multiplet's eigenfunction. $a = [-\ell(\ell+1)/3]c$ in order to satisfy the diagonal sum rule [*Gilbert*, 1971]. *Dahlen and Sailor* [1979] have calculated second-order effects of rotation that contribute to a and c. These second-order effects violate the diagonal sum rule. We expect a variational or Galerkin principle to replicate the perturbation terms. *Park* [1985] shows that first-order splitting of singlets within an isolated multiplet, when calculated with the linear eigenvalue formulation (39) or (56), gives a second-order Coriolis interaction that differs in sign with the *Dahlen and Sailor* [1979] value. The more accurate quadratic eigenvalue formulation (26) or (51) gives the correct sign for this term, which is proportional to b^2m^2. Examination of the values of a, b, c compiled in Table 1 of *Dahlen and Sailor* [1979] shows that this can be a problem for a handful of modes. The b^2m^2 term for ${}_0S_2$ is roughly equal to the cm^2 term. ${}_0S_3$, ${}_2S_1$, ${}_0S_4$, ${}_1S_2$, ${}_1S_3$, ${}_1S_4$, ${}_0T_2$, and ${}_1T_1$ all experience enough rotational splitting for $b^2 \gtrsim 0.03c$. However, outside this small group of grave, low angular order multiplets, the effect on the sign of b^2m^2 second-order Coriolis term caused by choosing the linear over the quadratic eigenvalue method will be negligible.

Finite dissipation does not change the above results, as one can generalize ${}_n\omega_\ell$, ${}_n\omega_\ell^m$, c, and a to be complex. Physical dispersion, however, generates additional second-order terms. We define $\nu_D = V_D({}_n\mathbf{s}_\ell^*, {}_n\mathbf{s}_\ell)$, where V_D is the dispersive functional introduced in (48). $V_D \ll ({}_n\omega_\ell)^2$ for all seismic free oscillations to the best of our knowledge. We solve (50) for the singlets of an isolated multiplet (n,ℓ) on a rotating, elliptical, attenuative-dispersive earth using the degenerate multiplet frequency ${}_n\omega_\ell = \hat{\omega}_0$ as the reference frequency. Using the quadratic eigenvalue scheme, the result, to second-order in small parameters, differs from (61) by a term linear in the nondispersive frequency perturbation:

$$\omega^m_{\text{dispersive}} \cong \omega^m_{\text{nondispersive}} \left[1 + \frac{\nu_D}{2\hat{\omega}_0^2} (a + bm + cm^2)\right] \tag{62}$$

where $\omega^m_{\text{nondispersive}}$ is given by (61). Since μ and κ increase logarithmically with frequency, ν_D is positive. Physical

TABLE 1. Comparison of Coupled-mode Singlet Frequencies

						${}_0S_2-{}_0T_3-{}_0S_4$		
	Observed	Dahlen and Sailor [1979]	Linear	Quadratic	Quadratic-Dispersive	Linear	Quadratic	Quadratic-Dispersive
${}_0S_2^{-2}$	0.3000100	0.299994	0.299776	0.300059	0.300053	0.299648	0.300046	0.299948
${}_0S_2^{-1}$	0.304799	0.304854	0.304633	0.304702	0.304699	0.304491	0.304682	0.304585
${}_0S_2^{0}$	0.309490	0.309548	0.309336	0.309336	0.309336	0.309194	0.309313	0.309219
${}_0S_2^{1}$	0.314000	0.314078	0.313865	0.313934	0.313936	0.313733	0.313913	0.313821
${}_0S_2^{2}$	0.318499	0.318442	0.318202	0.318468	0.318473	0.318089	0.318455	0.318365
$a(\times 10^{-3})$	0.117	0.376	−0.311	−0.310	−0.311	−0.771	−0.384	−0.689
$b(\times 10^{-3})$	14.924	14.905	14.893	14.882	14.891	14.906	14.882	14.889
$c(\times 10^{-3})$	−0.1757	−0.2671	−0.2802	−0.0586	−0.0589	−0.2627	−0.0506	−0.0503

All frequencies in mHz; ${}_0f_2^0 = 0.309432$ mHz.

dispersion therefore amplifies any deviation from the multiplet frequency, causing a larger multiplet splitting width overall. If attenuation is restricted to splitting within a single multiplet, this effect will be negligible for seismic modes, excluding perhaps the Slichter mode ${}_1S_1$. If (62) is compared with (47), the amplification factor for dispersive first-order splitting of a mode with quality factor Q is $1+\epsilon$, where $\epsilon \approx 2\Delta\omega/(\pi\omega Q)$ and $\Delta\omega/\omega$ is the relative splitting width of the multiplet. Even a strongly split mode like ${}_0S_2$ ($\Delta\omega \approx 18\,\mu$Hz) has $\epsilon < 10^{-4}$.

The dispersive effect can be modeled in the linear eigenvalue scheme as well, but care must be taken with the linear term in frequency. The function $f_Q(\omega) = (2\hat{\omega}_0)^{-2}(\omega^2 - 4\omega\hat{\omega}_0 + 3\hat{\omega}_0^2)$ is the polynomial in ω that multiplies the dispersive term in (50). If we approximate $4\omega\hat{\omega}_0 \approx 2\omega^2 + 2\hat{\omega}_0^2$, we obtain an alternative $f_L(\omega) = (\hat{\omega}_0)^{-2}(\hat{\omega}_0^2 - \omega^2)$ without a linear term. The difference $f_Q - f_L = (\hat{\omega}_0)^{-2}(\omega - \hat{\omega}_0)^2$, so that $f_Q'(\hat{\omega}_0) = f_L'(\hat{\omega}_0) = -1$, where the prime indicates first derivative. If we use $f_L(\omega)$ in place of $f_Q(\omega)$, the eigenfrequencies in the presence of dispersion differ from the eigenfrequencies in the absence of dispersion by the same factor derived for the quadratic eigenvalue scheme, to second-order. Therefore (62) applies for both methods of solving the matrix problem.

Quadratic and dispersive effects are not limited to the splitting of isolated multiplets. If mode coupling extends over a wide frequency band, these effects can increase. Moreover, eigenvectors are usually more sensitive than eigenvalues to matrix perturbations. Large errors in eigenvectors can seriously contaminate synthetic seismograms generated by coupled free oscillations, as will be shown in a later section. We performed several numerical experiments with an aspherical earth model to assess the possible problems. We have used model 1066A as the unperturbed model in these calculations. Model 1066A is nondispersive, i.e., it was derived from free oscillation frequencies without taking physical dispersion into account. The dispersive effect in the Galerkin procedure is a relative effect that depends on the bandwidth defined by the basis set singlets. We therefore expect that a nondispersive earth model is adequate to describe the effect of dispersion on coupling. We used the transition zone anomaly suggested by *Masters et al.* [1982] to produce large-scale coupling of singlets within multiplets.

We have compared quadratic and quadratic-dispersive eigenvalue procedures with the linear eigenvalue approximation for Galerkin basis sets consisting of the singlets of the multiplet groups ${}_0S_2$, ${}_0S_2-{}_0T_3-{}_0S_4$, ${}_3S_1-{}_1S_3$, ${}_0S_{11}-{}_0T_{12}$, ${}_0S_{19}-{}_0T_{20}$, ${}_0S_{32}-{}_0T_{31}$, and ${}_0S_{12}-{}_0T_{13}-{}_0S_{14}-{}_0T_{15}-{}_0S_{16}$. The first three groups are very low frequency, with coupling dominated by rotation. The next three groups are quasi-degenerate pairs of the $(l,l+1)$, $(l,l-1)$ crossovers of the fundamental spheroidal and toroidal mode branches. The last group is a chain of fundamental modes coupled by rotation over a frequency range of 0.475 mHz, with a relative $\Delta\omega/\omega > 20\%$. Secular modes have been excluded from the calculations. Only the gravest modes are significantly affected by the exclusion. We report in detail the ${}_0S_2$ calculation and those using the last two groups. The other calculations gave similar results, which are summarized by *Park* [1985].

${}_0S_2$

Since the Slichter mode ${}_1S_1$ is virtually confined to the core and remains unobserved [*Rydelek and Knopoff*, 1984], ${}_0S_2$ is the gravest observed seismic free oscillation. The Chandler wobble, though technically a terrestrial free oscillation [*Smith and Dahlen*, 1981], is not primarily seismic. Measurements of all five singlets of ${}_0S_2$ have been reported using spherical harmonic stacking [*Buland et al.*, 1979] and multitaper spectral techniques (J. Park *et al.*, unpublished manuscript, 1986). Measurements from both studies suggest the ability to resolve frequencies to within 0.1 μHz with International Deployment of Accelerometers (IDA) seismic data from a great earthquake, in this case the Sumbawa event of 1977. In Table 1 we compare singlet frequencies from the *Buland et al.* [1979] study with frequencies computed from rotation and hydrostatic ellipticity using various schemes, including the results of *Dahlen and Sailor* [1979], obtained through perturbation techniques. The values of the first-order splitting parameters (i.e., for ${}_0\omega_2^m = {}_0\omega_2(1+a+bm+cm^2)$) were obtained by fitting a quadratic to the singlet frequencies in all but the Dahlen and Sailor case, where their values are given. All values are given with respect to the degenerate multiplet frequency of ${}_0S_2$ appropriate to model 1066A.

There is considerable variation of a and c among coupling schemes. The linear splitting term b varies only slightly. All values for the constant shift a gotten through the chosen coupling schemes are opposite in sign compared to both observation and the Dahlen and Sailor

value. The latter calculations included coupling perturbations from secular modes. These effects, discussed by *Park* [1985], will increase the mean multiplet frequency. In the cases where ${}_0S_2$ couples to nearby modes ${}_0S_4$ and ${}_0T_3$, the static shift is somewhat amplified, but much less so in the quadratic coupling scheme. The large negative a for the quadratic-dispersive scheme is due to an artificial shift in the shear and bulk moduli of 1066A caused by arbitrarily specifying its fiducial frequency $\hat{\omega}_0$ to lie between those of the three coupled multiplets ${}_0S_2$, ${}_0T_3$, ${}_0S_4$. On a dispersive earth model $\hat{\omega}_0$ would be fixed for all modes, with dispersive corrections to the degenerate eigenfrequencies preincorporated. Relative spacing of singlets in ${}_0S_2$ is relatively unaltered by the dispersive scheme. The various shortcomings of the linear eigenvalue approach cancel in such a way as to have its value for the quadratic coefficient c be roughly equivalent to the Dahlen and Sailor value. The nominally more precise quadratic approaches give values of c that differ strongly, but the effect of secular modes is not included. Galerkin calculations in which secular modes are included match the observed frequencies better than any of the calculations tabulated here [*Park*, 1985].

${}_0S_{32} - {}_0T_{31}$

This multiplet pair, in all standard earth models derived from free oscillation data, marks the crossing of the ${}_0S_\ell - {}_0T_{\ell-1}$ dispersion branches. As the highest-frequency fundamental branch crossing susceptible to Coriolis force, the 128 singlets of this multiplet pair couple and split in a dramatic fashion. The effects of rotation, ellipticity, and the *Masters et al.* [1982] anomaly were included in comparative calculations. The hybrid singlet frequencies span a bandwidth of roughly 20 μHz, clustering in real-part frequency in the center of the band (cf. Figure 11).

A comparison between quadratic and linear eigenproblems yields larger discrepancies in hybrid singlet composition than in other examples. Eleven of 128 singlets of the quadratic eigenproblem solution, in the central cluster, differ by more than 10^{-3} in composition. Four singlets vary by 1–2%. The absence of larger discrepancies, however, is almost surprising in light of the profound hybridization and nonorthogonality of the coupled singlet eigenfunctions (cf. Figures 12 and 13). A large number of hybrid singlet compositions differ by only one decimal place greater than the numerical eigenvector precision. Results for the quadratic-dispersive eigenproblem scheme are similar, with 14 singlet compositions differing by greater than 10^{-3} and four singlets with discrepancies between 1 and 1.5%. Frequency discrepancies between schemes are no larger than the width of the quadratically coupled singlet band which widens by 0.003 μHz relative to the linearly coupled band, while the dispersively coupled band widens by 0.07 μHz. In only one case does a pair of hybrid singlets switch position in relative real-part frequency. None of these discrepancies is likely to be readily observable in seismograms.

${}_0S_{12} - {}_0T_{13} - {}_0S_{14} - {}_0T_{15} - {}_0S_{16}$

This chain of low-frequency fundamental modes couples principally through Coriolis force. The degenerate frequencies of these modes (using model 1066A) are widely spaced:

$$ {}_0f^S_{12} = 1.989000 \text{ mHz} $$
$$ {}_0f^T_{13} = 1.979013 \text{ mHz} $$
$$ {}_0f^S_{14} = 2.229991 \text{ mHz} $$
$$ {}_0f^T_{15} = 2.212406 \text{ mHz} $$
$$ {}_0f^S_{16} = 2.456930 \text{ mHz} $$

However, the Coriolis coupling is strong enough to induce component mixtures of up to 5% in relative amplitude between modes $\gtrsim 0.2$ mHz apart in degenerate frequency. The maximum energy admixture would be roughly $(0.05)^2 = 0.25\%$. Effects on frequency and attenuation would likely be smaller than those on amplitudes. With coupling evident across large frequency spacings, it is prudent to consider the approximation made by taking an intermediate fiducial frequency ω_0 for Coriolis interaction terms in the linear eigenproblem approach. Comparison calculations were made using rotation, ellipticity and the *Masters et al.* [1982] model.

Significant discrepancies between schemes were noted in these tests. Although hybrid singlet frequencies were, on the whole, relatively stable, isolated singlet discrepancies were as large as 0.1 μHz, with most discrepancies hovering between $\pm 0.03\,\mu$Hz. Quadratic and quadratic-dispersive singlet frequencies were on average slightly higher relative to linear eigenproblem frequencies due to the correct sign of the second-order Coriolis term $\frac{1}{2}b^2m^2$. In isolated cases, pairs of singlets appear to have coupled differently in the different schemes, leading to a relative frequency repulsion/attraction of $\sim 0.15\,\mu$Hz and a 1–10% variation in hybrid component mixture. Isolated discrepancies of relative component mixture of up to 30% can be found between the linear and quadratic-dispersive eigenproblem solutions, but this occurs principally from the remixing of nearly degenerate ($\Delta\omega \lesssim 0.02\,\mu$Hz) singlets. In the quadratic-linear comparison, 43 of 145 singlet comparisons varied in composition by more than 1%, 12 of these 43 varied by more than 5%. However, in the middle two hybrid multiplets ${}_0St_{14}$, ${}_0Ts_{15}$, only four hybrid singlets varied by more than 1%, and no one singlet comparison varied by more than 4%. In the quadratic-dispersive linear comparison, 55 of 145 singlet comparisons varied by more than 1%, with 18 of these 55 varying by more than 5%. The 18 worst cases occur in nine nearly degenerate pairs of hybrid singlets. Eight of 60 hybrid singlets in ${}_0St_{14}$, ${}_0Ts_{15}$ possess variations greater than 1%. Hybrid singlet attenuation varies by a few percent between schemes. This variation is caused principally by the swapping of spheroidal and toroidal components between nearly degenerate singlets. Since the toroidal spherical earth singlets have an intrinsic Q that is roughly half that of the spheroidal singlets, first-order perturbations in relative composition result in first-order variations in singlet Q. If averaged over many neighboring singlets, these variations will tend to cancel and thus be unobservable.

Although substantial numerical variation exists between coupling schemes in this example, it is offset largely by averaging the effects over neighboring singlets. This

averaging is unavoidable for surface wave modes, as individual singlets, broadened by attenuation and packed densely into hybrid multiplets, are unresolvable. Moreover, differences between calculation schemes are much smaller for hybrid singlets near the center of the basis set bandwidth. Hybrid modes at the frequency extremes of a large basis set are relatively unreliable as coupling effects from outside the bandwidth are omitted. That they are also less reliable in the linear eigenproblem approximation to the full quadratic or dispersive eigenproblem should not cause great additional concern. A prudent large-scale coupling scheme will retain hybrid singlets from the central frequency region of each calculation, using overlapping basis sets. However, as the coupling calculations become more ambitious and if our knowledge of lateral structure becomes as precise as our current knowledge of radial structure, the use of dispersive earth models like PREM [*Dziewonski and Anderson*, 1981] becomes necessary, and the approximations made in neglecting eigenproblems of order higher than linear may have some impact at frequencies greater than 1 mHz. At lower frequencies, the gravest modes will be influenced somewhat by the earth's secular modes of motion which, in a Galerkin formalism, can only be properly modeled with a quadratic or higher-order eigenproblem.

6. Numerical Tests of Galerkin Procedure: Nonorthogonal Eigenvectors

Care must be taken in the solution of the initial value problem (e.g., fault displacement at $t = 0$) for seismic motion on an aspherical attenuative earth. In simple mechanical systems one finds the "normal" modes of oscillation directly from the configuration. The earth's "normal" modes, as they are often called, are truly orthogonal only on the particular density structure from which they are derived. As can be seen from the dissipative coupled pendulum problem, the free modes of an attenuative system need not be orthogonal under either the standard Euclidean norm or the inner product defined by the kinetic energy interaction matrix. The Galerkin procedure outlined in this paper uses the set of normal modes appropriate to a given terrestrial monopole to describe seismic motion on a more complicated model. The hybrid free oscillations that result are no longer normal. Even if the earth model is nonattenuative, a perturbation in density structure will cause nonorthogonality with respect to the sperhically averaged density structure. If referenced to the perturbed rather than the spherically averaged density structure, the new modes will be "normal" in a nonattenuative model. For computational purposes, it is useful to separate the effects of variable attenuation rate and density perturbation. We will find that the former effect is often quite large, while the latter is usually small enough to be neglected.

We return to the similarity decomposition of the modified potential energy matrix $\tilde{\mathbf{V}}'$:

$$\tilde{\mathbf{V}}' = \mathbf{S} \cdot \mathbf{D} \cdot \mathbf{S}^{-1} \tag{63}$$

After some experimentation we have found the EISPACK subroutine path CBAL-CORTH-COMQR2-CBABK2 to be more desirable than other algorithms. We can relate the matrix decomposition (63) to the source excitation formula (60) by noting that $\alpha_{ki} = (\mathbf{L}^{-H} \cdot \mathbf{S})_{ik}$ and $\beta_{ki} = (\mathbf{S}^{-1} \cdot \mathbf{L}^{-1})_{ki}$, where $\mathbf{L}$ is defined in (54). The COMQR2 subroutine path computes the matrix of right-eigenvectors $\mathbf{S}$, after which a back transform using the Cholesky factor of $\mathbf{T}$ obtains $\mathbf{L}^{-H} \cdot \mathbf{S}$. The explicit calculation of $\mathbf{S}^{-1}$ is both time consuming and potentially unstable. Close examination of (60) shows that neither $\mathbf{S}$ or $\mathbf{S}^{-1}$ are required explicitly, only the quantities $\boldsymbol{\gamma}_R \cdot (\mathbf{L}^{-H} \cdot \mathbf{S})$ and $\mathbf{S}^{-1} \cdot \mathbf{L}^{-1} \cdot \boldsymbol{\gamma}_S$, where $(\boldsymbol{\gamma}_S)_i = \mathbf{M}(\omega) \cdot \boldsymbol{\epsilon}_i(\mathbf{r}_o)$, the excitation at r_o of the ith spherical earth singlet, and $(\boldsymbol{\gamma}_R)_i = \hat{\mathbf{x}} \cdot \mathbf{s}_i(\mathbf{r})$ is the displacement of the ith spherical earth singlet at the receiver location $\mathbf{r}$ in the direction specified by the unit vector $\hat{\mathbf{x}}$. The synthesis of three-component seismic motion requires three orthogonal choices for $\hat{\mathbf{x}}$ and thus three distinct $\boldsymbol{\gamma}_R$ "receiver vectors." In order to compute the vector-valued hybrid source excitations using $\mathbf{S}^{-1}$, we use the LU decomposition of $\mathbf{L}^{-H} \cdot \mathbf{S}$:

$$\mathbf{L}^{-H} \cdot \mathbf{S} = \mathbf{P} \cdot \mathbf{W} \cdot \mathbf{U} \tag{64}$$

where $\mathbf{W}$ is lower triangular with diagonal elements $W_{ii} = 1$, $\mathbf{U}$ is upper triangular, and $\mathbf{P}$ is a permutation matrix $P_{ij} = \delta_{\pi(i)j}$ where $\pi(i)$ is the permutation of rows. $\mathbf{P}$ represents a partial pivoting scheme necessary to stabilize the numerical decomposition. The LU decomposition is the usual first step in explicitly calculating the inverse of a matrix. For our purposes we need go no further. Note that

$$(\mathbf{L}^{-H} \cdot \mathbf{S})^{-1} = \mathbf{S}^{-1} \cdot \mathbf{L}^{H} = \mathbf{S}^{-1} \cdot \mathbf{L}^{-1} \cdot \mathbf{L} \cdot \mathbf{L}^{H} = \mathbf{S}^{-1} \cdot \mathbf{L}^{-1} \cdot \mathbf{T} \tag{65}$$

The kinetic energy interaction matrix $\mathbf{T}$ is very close to the identity matrix $\mathbf{I}$, and so tempts us to ignore it. If we take $\mathbf{T} - \mathbf{I}$ to be negligible, we have approximated

$$\mathbf{S}^{-1} \cdot \mathbf{L}^{-1} \cong \mathbf{U}^{-1} \cdot \mathbf{W}^{-1} \cdot \mathbf{P}^{-1} \tag{66}$$

from which $\mathbf{S}^{-1} \cdot \mathbf{L}^{-1} \cdot \boldsymbol{\gamma}_S \cong \mathbf{U}^{-1} \cdot \mathbf{W}^{-1} \cdot \mathbf{P}^{-1} \cdot \boldsymbol{\gamma}_S$ can be calculated by reordering indexes and performing two complex back transforms, at a cost of N^2 complex multiplications and additions. The number of operations required by the two back transforms equals that required for the forward transform

$$\gamma_R \cdot \mathbf{L}^{-H} \cdot \mathbf{S} = \gamma_R \cdot \mathbf{P} \cdot \mathbf{W} \cdot \mathbf{U}$$

and can be vectorized since the inner loop is not recursive. One obvious advantage of the LU decomposition scheme is that it stores both $\mathbf{L}^{-H} \cdot \mathbf{S}$ and its inverse in the same matrix plus an integer vector that stores the row permutation $\pi(j)$. The exact calculation can be gotten as well by extending the formalism, noting that

$$\begin{aligned} \mathbf{S}^{-1} \cdot \mathbf{L}^{-1} &= (\mathbf{L}^{-H} \cdot \mathbf{S})^{-1} \cdot \mathbf{L}^{-H} \cdot \mathbf{L}^{-1} \\ &= \mathbf{U}^{-1} \cdot \mathbf{W}^{-1} \cdot \mathbf{P}^{-1} \cdot \mathbf{L}^{-H} \cdot \mathbf{L}^{-1} \end{aligned} \tag{67}$$

The approximation (66) can be removed with two additional back transforms using the Cholesky factors of $\mathbf{T}$, of which only one need be stored. We will later discuss a numerical comparison test of (66) and (67).

It is useful to examine a few examples of coupled modes in order to assess the impact of the nonorthogonality of hybrid singlets. In Figures 5—7 we show the results

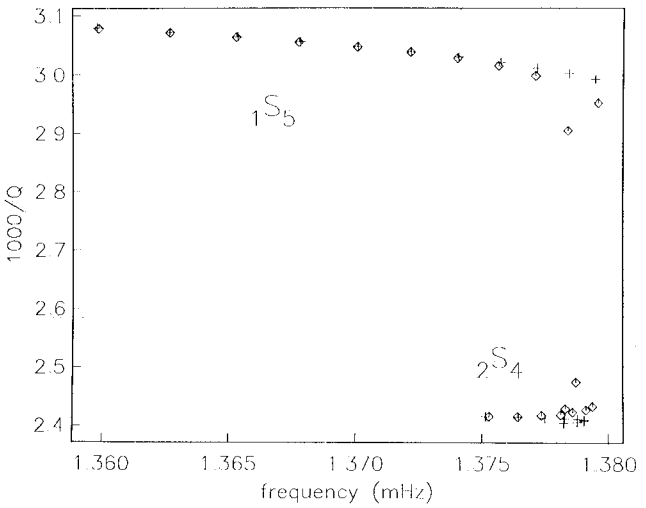

Fig. 5. Hybrid singlet frequencies of $_2S_4$–$_1S_5$ before and after coupling. Pluses indicate the real-part frequencies and $1000/Q$ values for the singlets of $_2S_4$ and $_1S_5$ self-split by rotation and ellipticity. Diamonds indicate the hybrid frequencies of $_2S_4$–$_1S_5$ coupled with model M84A of *Woodhouse and Dziewonski* [1984]. All calculations use model 1066A [*Gilbert and Dziewonski*, 1975] for the underlying spherical earth structure.

of coupling $_2S_4$ and $_1S_5$ through the aspherical upper mantle shear velocity model M84A proposed by *Woodhouse and Dziewonski* [1984]. Figure 5 shows the effect of the laterally varying model on complex-valued singlet frequencies. In this and later such figures the pluses indicate spherical harmonic singlet frequencies plotted in millihertz versus $1000/Q$ appropriate for a first-order splitting by rotation and ellipticity. Although the real-part frequencies can split widely, the radial Q model fixes the imaginary-part frequency at the degenerate multiplet value, leading to a noticeable drift in values of $1000/Q = 2000[\mathrm{Im}(\omega)/\mathrm{Re}(\omega)]$. The even spacing of the singlet frequencies of $_1S_5$ indicate strong rotational splitting. The clustered singlets of $_2S_4$ reflect predominately ellipticity splitting. The diamonds show the hybrid singlet frequencies. Coupling between multiplets manifests itself in this type of figure by the "attraction" of opposing singlet attenuation rates toward an average value of $1000/Q$. In Figure 5 we see that a few singlets of the lower Q, rotationally split $_1S_5$ have interacted with the cluster of less attenuative $_2S_4$ singlets. Due to angular selection rules, this coupling is caused by odd-order components in the lateral model. In Figure 6 the coupling coefficients in this problem are symbolically graphed, using a sequence of thresholds to indicate the magnitude of the matrix elements $(\mathbf{L}^{-H}\cdot\mathbf{S})_{ij}$. With the $\boldsymbol{\alpha}_k$ normalized so that $\boldsymbol{\alpha}_k^*\cdot\boldsymbol{\alpha}_k = 1$, coefficient positions with magnitudes less than 0.05 were left blank. Each column of the graph represents the expression of a hybrid singlet in terms of spherical earth (i.e., spherical harmonic) singlets. The hybrid singlets are ordered by increasing real-part frequency. Most of the singlets of $_1S_5$ remain virtually uncoupled under the influence of Woodhouse-Dziewonski model M84A. The singlets of $_2S_4$ not only couple with the $m = 3,4,5$ singlets of $_1S_5$ through the odd-order lateral structure but also couple strongly among themselves through the even-order lateral structure.

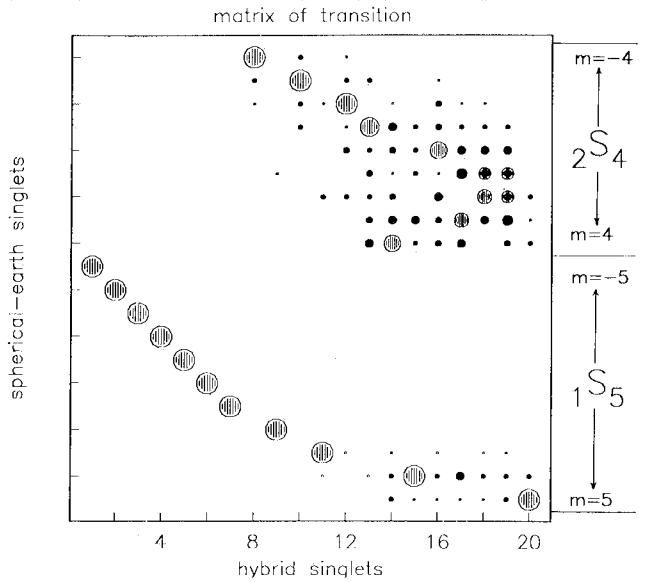

Fig. 6. Schematic of hybrid $_2S_4$–$_1S_5$ coupled singlets in terms of spherical harmonic singlets $_nS_l^m$, using rotation, ellipticity, and model M84A. The symbols show the relative magnitude of the matrix elements of the matrix of transition S defined by (65). Values for which $|(\mathbf{S})_{ij}| < 0.05 \max(ij)\{|(\mathbf{S})_{ij}|\}$ are omitted from the plot. Each column represents the linear combination of spherical harmonic singlets that constitutes the jth hybrid singlet particle motion, ordered by increasing frequency. Each row represents the distribution of an individual spherical earth singlet among the coupled hybrid singlets. Symbol size indicates relative magnitude. Note that the spherical-earth singlets $_1S_5^m$, $-5 \leqslant m \leqslant 2$, remain virtually uncoupled but that the $m = 3,4,5$ singlets of $_1S_5$ couple significantly among themselves and with the singlets of $_2S_4$. Hybrid singlets dominated by $_1S_5^m$, $m = 3,4,5$, particle motion show noticeable perturbations in $1000/Q$ in Figure 5.

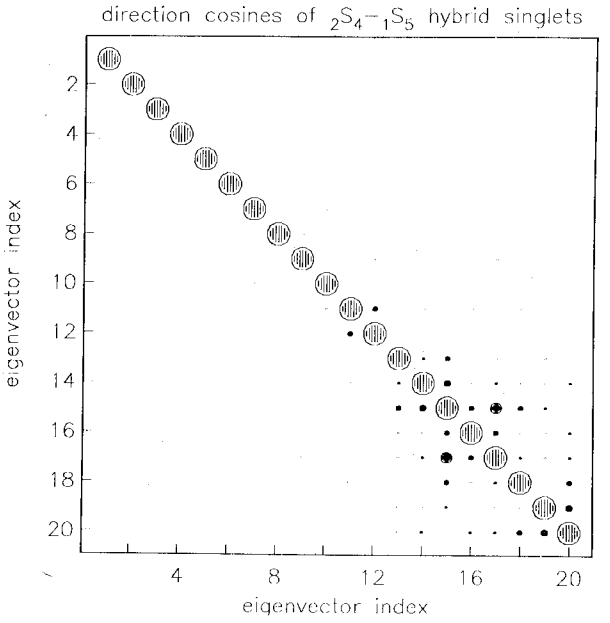

Fig. 7. Direction cosines of the right-eigenvectors that define the hybrid singlets of $_2S_4$–$_1S_5$, coupled with rotation, ellipticity, and M84A. This matrix of direction cosines is found by forming $\boldsymbol{\Gamma} = \mathbf{S}^H\cdot\mathbf{S}$, where $\mathbf{S}$ is defined by (65) and normalizing the rows and columns so that $\Gamma_{ii} = 1$. Values of $|\Gamma_{ij}| < 0.01$ are not plotted. The magnitudes of Γ_{ij} are indicated by symbol size. If the right eigenvectors of the coupling interaction matrix system were orthonormal, $\boldsymbol{\Gamma} = \mathbf{I}$ the identity matrix.

The nonorthogonality of the hybrid singlets can be demonstrated by computing $\Gamma_{ij} = \boldsymbol{\alpha}_i^* \cdot \boldsymbol{\alpha}_j$, the complex-Hermitian Gram matrix of eigenvectors. The magnitudes of the off-diagonal elements of Γ_{ij} represent the direction cosines between the hybrid free oscillations of the perturbed earth model, as long as the diagonal elements are normalized so that $\Gamma_{ii} = 1$. If the $\boldsymbol{\alpha}_i$ were orthonormal, all $\Gamma_{ij} = 0$ for $i \neq j$. The complex Gram matrix for the coupled singlets of ${}_2S_4 - {}_1S_5$ is symbolically graphed in Figure 7, with values of $|\Gamma_{ij}| < 0.01$ (corresponding to $\lesssim 0.57°$ deflection from the perpendicular in complex 20 space) left blank. Noticeable nonorthogonality afflicts only a handful of hybrid singlets, but one pair of hybrid singlet eigenvectors, $\boldsymbol{\alpha}_5$ and $\boldsymbol{\alpha}_7$, deviate over 15° from the perpendicular with respect to each other.

The largest coupling that has been observed thus far in free oscillation data occurs between fundamental spheroidal and toroidal multiplets and is caused principally by Coriolis force [*Masters et al.*, 1983]. Angular selection rules [*Dahlen*, 1968] restrict coupling to spheroidal and toroidal multiplet pairs that differ by one in angular order. There is also allowable coupling between distinct like-type multiplets of equal angular order, but this effect is much smaller. One example of spheroidal-toroidal coupling through Coriolis force and lateral structure is given in Figures 8–10 for the multiplet pair ${}_0S_{14} - {}_0T_{15}$. Figure 8 shows singlet frequencies both before (using first-order splitting of rotation and ellipticity) and after coupling through rotation, ellipticity, and the $s = 2$ transition zone model suggested by *Masters et al.* [1982]. The hybrid singlets remain grouped into separate hybrid multiplets, dubbed *St* and *Ts* modes by *Masters et al.* [1983], according to which variety of particle motion predominates. Close inspection reveals that the two "centers of mass" of the hybrid multiplets have come closer in attenuation rate but have repelled in real-part frequency. The symbolic representation of the components of the resultant hybrid singlets is given in Figure 9. As in Figure 6, the columns

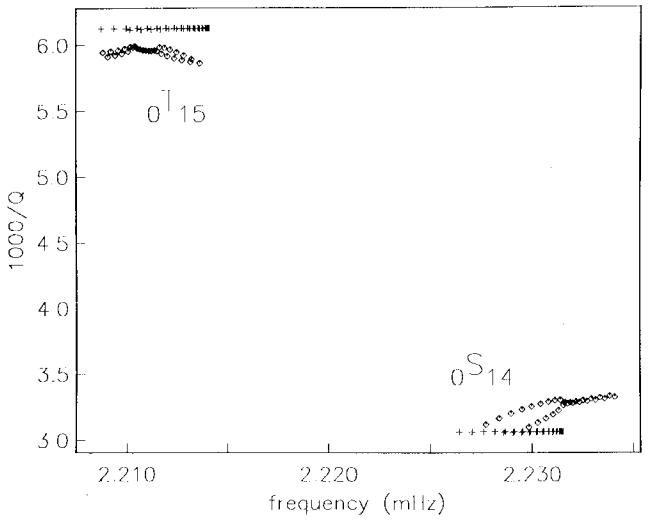

Fig. 8. Singlet hybrid frequencies for ${}_0S_{14}$–${}_0T_{15}$. The pluses indicate the real-part frequency $1000/Q$ values for spherical harmonic singlets self-split by rotation and ellipticity, with coupling between ${}_0S_{14}$ and ${}_0T_{15}$ neglected. The diamonds indicate hybrid eigenfrequencies for coupling due to rotation, ellipticity, and the $\ell = 2$ transition zone model suggested by *Masters et al.* [1982].

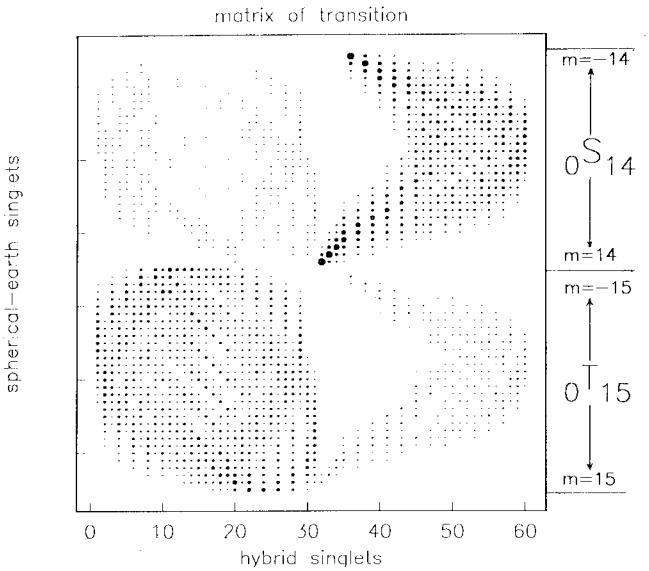

Fig. 9. Schematic of hybrid ${}_0S_{14}$–${}_0T_{15}$ singlets in terms of spherical harmonic singlets ${}_nS_\ell^m$, ${}_nT_\ell^m$ coupled with rotation, ellipticity, and the $\ell = 2$ transition zone model. Symbol conventions identical to those of Figure 6.

of the graph represent the component parts of the hybrid singlets, ordered in increasing real-part frequency. The spherical earth singlets, referenced by row, are grouped into separate multiplets within which ordering is by azimuthal order m. The symbolic representation of the Gram matrix $\Gamma_{ij} = \boldsymbol{\alpha}_i^* \cdot \boldsymbol{\alpha}_j$ is shown in Figure 10. Nonorthogonality is confined mostly to hybrid singlets that lie close together in frequency but afflicts nearly all hybrid singlets to some extent. Values of $|\Gamma_{ij}| < 0.05$ (corresponding to $\lesssim 2.87°$ deflection from the perpendicular) were left blank.

The most profound example of nonorthogonal hybrid singlet oscillations that we have found at frequencies $\leqslant 5$ mHz is the fundamental multiplet pair ${}_0S_{32} - {}_0T_{31}$. This pair represents the third, highest-frequency crossing of the ${}_0S_\ell$ fundamental Rayleigh wave dispersion branch with either the ${}_0T_{\ell+1}$ or ${}_0T_{\ell-1}$ branches and the most dramatic example of coupling through Coriolis force. The study of *Masters et al.* [1983] has cast doubt on the placement of the branch crossing at exactly ${}_0S_{32} - {}_0T_{31}$, and future measurements and models may realign the branches. However, this coupling case serves as a useful numerical example of the worst case complications of large-scale coupling of neighboring singlets. We have used the $s = 2$ transition zone lateral structure to couple the 128 singlets of the two multiplets. Figure 11 shows the singlet frequencies before and after the coupling calculation. As in Figure 5, the pluses represent first-order splitting of frequencies due to ellipticity and rotation. The diamonds are placed at singlet frequencies, in millihertz versus $1000/Q$, derived from the full calculation. The attraction of attenuation rate and the repulsion of oscillation frequency, characteristic of attenuative coupling, are evident in varying degrees among the hybrid singlets. First-order rotational splitting is comparatively weak for these multiplets. The tendency for the singlet frequencies in Figure 11 is to group in pairs of singlets with nearly arithmatically opposite azimuthal components. The traveling wave explica-

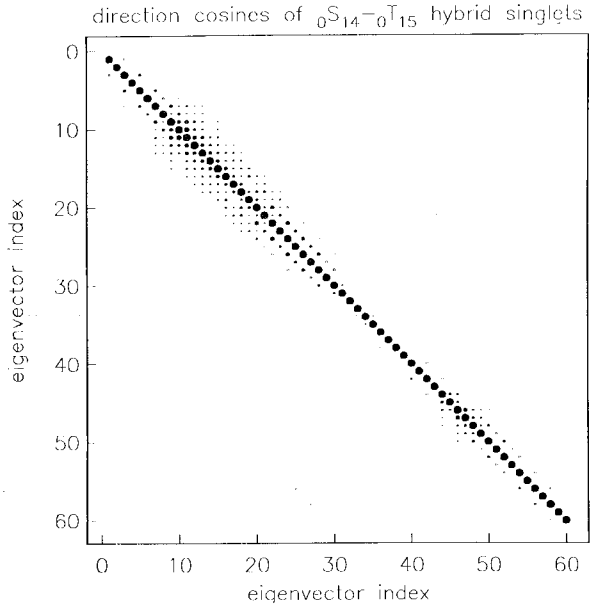

Fig. 10. Direction cosines of the right-eigenvectors that define the hybrid singlets of $_0S_{14}$–$_0T_{15}$, coupled with rotation, ellipticity, and the $\ell = 2$ transition zone model. Symbol conventions identical to those of Figure 7. Values of $|\Gamma_{ij}| < 0.05$ are not plotted.

tion of this effect is that the associated surface wave cannot tell the difference between traveling east to west and west to east. A rougher lateral structure, like M84A of *Woodhouse and Dziewonski* [1984], causes more interaction between $\pm m$ singlets, disrupting this pairing of hybrid frequencies. The thorough scattering of eigenfrequencies in the figure suggests that it would be difficult in this case to separate the singlets into a quasi-spheroidal and quasi-toroidal hybrid multiplets. The coupling matrix, symbolically graphed in Figure 12, also offers little help in distinguishing separate hybrid multiplets.

The Gram matrix of the hybrid singlets of $_0S_{32} - {}_0T_{31}$ is graphed symbolically in Figure 13. The degree of nonorthogonality is large. Two hundred and eighty-five eigenvector pairings out of 8128 have direction cosine $\geqslant 0.5$ ($\geqslant 30°$ deflection from the perpendicular) and 30 pairs have direction cosine $\geqslant 0.9$ ($\geq 65°$ deflection). Moreover, smaller-scale nonorthogonality afflicts nearly all eigenvectors.

The degree of nonorthogonality between hybrid singlets on an attenuative earth model varies with the strength of coupling and the amount of attenuation attraction between multiplets of varying attenuation rates. Most of the coupling calculations reported by *Masters et al.* [1983] involve comparatively small amounts of nonorthogonality. Considering the cost of computing the LU decomposition to represent both left and right eigenvectors of the interaction Lagrangian matrix, it is germane to ask whether adequately precise seismograms can be synthesized by approximating

$$\mathbf{S}^{-1} \cdot \mathbf{L}^{-1} \cong \mathbf{S}^{H} \cdot \mathbf{L}^{-1} = (\mathbf{L}^{-H} \cdot \mathbf{S})^{H} \tag{68}$$

We can compare (68) with calculations using either (66) or (67) in order to assess the relative error invoked in neglecting the Cholesky back transforms implicit in (67). For this experiment we calculated coupling due to rotation, ellipticity, and the lateral structure of *Woodhouse and Dziewonski* [1984] for all spheroidal and toroidal fundamental mode multiplets, grouped in distinct batches of 44 to 174 singlets, with degenerate frequency < 6.2 mHz. The matrix decompositions were performed on the Cray 1A machine at the National Magnetic Fusion Energy Computer Center at the Lawrence Livermore National Laboratory. Later calculation of seismograms was performed on the PRIME 750 machine, equipped with an FPS-AP120B array processor, at the Scripps Institution of Oceanography. We compared seismograms for a suite of source-receiver pairs, using a variety of source orienta-

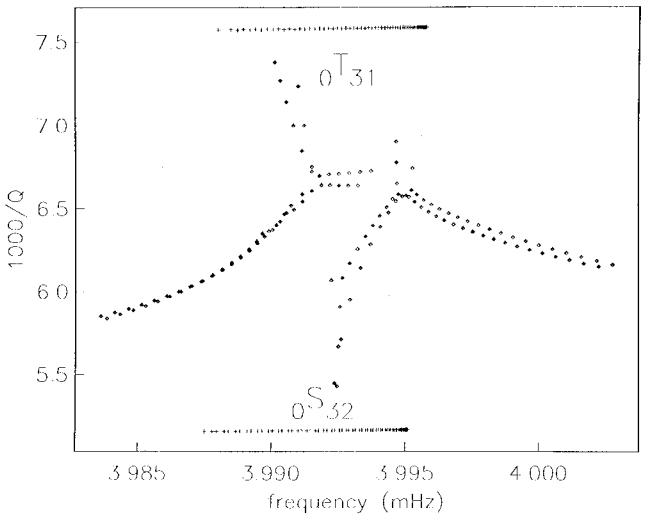

Fig. 11. Hybrid singlet frequencies for $_0S_{32}$–$_0T_{31}$. The plus markers indicate the real-part frequency. $1000/Q$ values for spherical harmonic singlets self-split by rotation and ellipticity, with coupling between $_0S_{32}$ and $_0T_{31}$ neglected. The diamonds indicate hybrid frequencies for coupling due to rotation, ellipticity, and the $\ell = 2$ transition zone model.

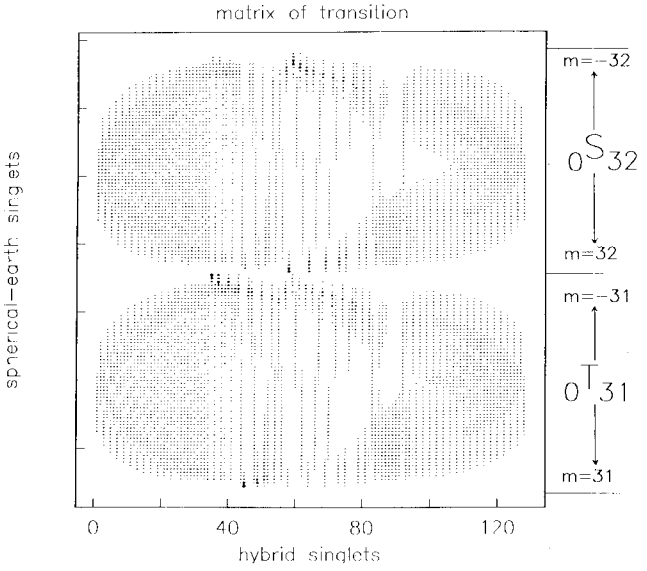

Fig. 12. Schematic of $_0S_{32}$–$_0T_{31}$ singlets in terms of spherical harmonic singlets, coupled by rotation, ellipticity, and the $\ell = 2$ transition zone model. Symbol conventions identical to those of Figure 6.

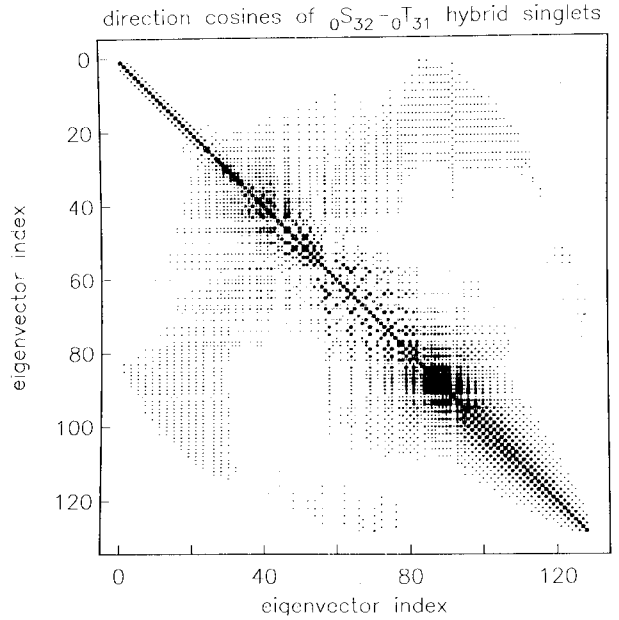

Fig. 13. Direction cosines of the right eigenvectors that define the hybrid singlets of $_0S_{32}$–$_0T_{31}$, coupled with rotation, ellipticity, and the $\ell = 2$ transition zone model. Symbol conventions similar to those of Figure 7. Values of $|\Gamma_{ij}| < 0.05$ are not plotted.

tions, for the exact representation (67), the simplified LU approach (66) and the Hermitian transpose approximation (68). A low pass filter was applied to the synthetic traces in order to reduce ringing from the edge of the frequency cutoff.

Figures 14–17 show synthetic seismograms for a seismic source at the hypocenter of the June 22, 1977, Tonga event (22.9°S, 175.9°W, depth 65 km). Strike-slip sources were used to increase the long-period toroidal mode excitation and thereby accentuate coupling effects. Figures 14 and 15 show IDA instrument response of NNA (Ñaña, Peru) and ALE (Alert, Northwest Territories), respectively, for a 50° strike, 90° dip, 0° slip source. The Tonga-ALE source receiver path is nearly polar, with principally north-south wave propagation. The great circle of the Tonga-NNA path is inclined only 26° above the equator, possessing mostly east-west wave propagation. On all traces the Rayleigh wave arrivals R_1 through R_6 can be observed. There is no visual difference between the exact representation and the simplified LU approach that omits the Cholesky factors. Differencing the records reveals variations on the order of 0.1–0.5% of the maximum amplitude of the record. The Hermitian transpose approximations are inadequate in both source-receiver orientations. Noncausal precursory motion, much larger than that attributable to band edge ringing, contaminates the start of both records. More sinister is the appearance of dubious phases (e.g., the small pulse just beyond R_2 in both ALE and NNA records).

Figures 16 and 17 show identical source-receiver pairs for a strike-slip event with 90° strike. The azimuth of the source-receiver path in both cases exits the source near the node of the Rayleigh wave radiation pattern and the antinode of the Love wave radiation pattern. As discussed by *Park* [1986], the Tonga-ALE geometry is especially favorable for Coriolis coupling effects, while the Tonga-NNA geometry is unfavorable. The NNA synthetics in Figure 16 show the first five Rayleigh wave packet arrivals clearly, with no discernible difference between the exact calculation and that omitting the Cholesky factor. Neglecting the dual basis in the Hermitian transpose approximation gives a very poor result, with considerable interpacket energy. In a case where coupling effects are strong (Figure 17), there is considerable interpacket energy in all calculation schemes, with poorly defined surface wave arrivals and unexpected phases. The exact and simplied LU calculations remain visually indistinguishable. The Hermitian transpose approximation leads to enormous precursory waveforms and waveforms whose phase differs greatly from that of the more precise calculations.

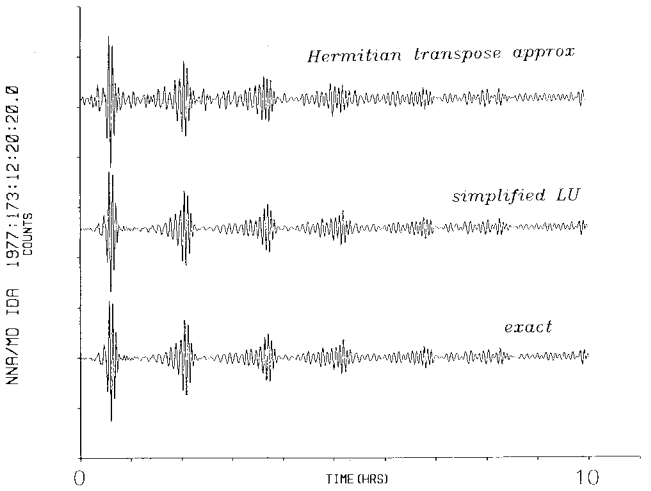

Fig. 14. Strike-slip synthetic source of 1977 Tonga hypocenter, as calculated for IDA station NNA using the three linear algebra algorithms discussed in text. The lower trace shows the exact calculation. The middle trace shows the simplified LU approach, which discards the effect of the kinetic energy matrix in the transformation of the source excitation vector $\boldsymbol{\gamma}_s$. The top trace shows the result of using the right eigenvectors of the coupling matrix rather than their dual left eigenvectors in the transformation of $\boldsymbol{\gamma}_s$. The lower traces are visually identical, while the upper trace has spurious complexity.

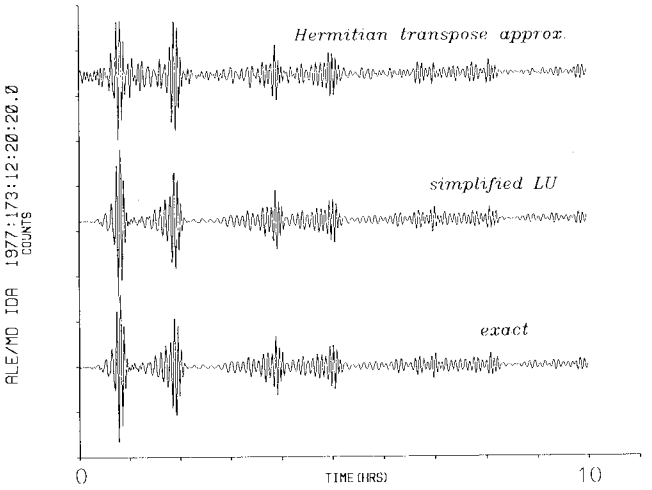

Fig. 15. Tonga-ALE seismograms for the same source taken in Figure 14. The upper trace has significant spurious waveform energy preceding R_1.

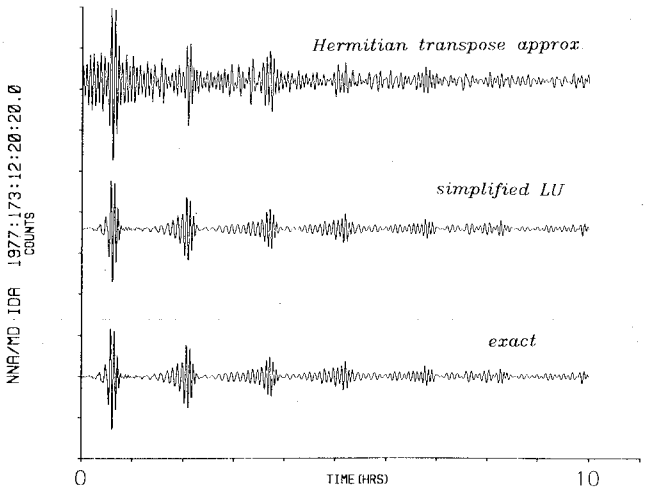

Fig. 16. Tonga-NNA seismograms for a strike-slip source with source strike oriented so as to enhance possible coupling effects. The lower traces show no visible effects, as would be expected on a roughly equatorial ($\Theta = 26°$) propagation path. The upper trace, which ignores eigenvector nonorthogonality in the source excitation, contains much spurious energy.

The case for using the dual-vector formalism in attenuative coupling calculations is unassailable. The simplified LU calculation scheme, which omits the Cholesky factors, appears adequate in the test calculations that have been done thus far. An enlargement of the first four hours of a synthetic with strong coupling effects (Tonga-SPA (south pole), 90° strike, 90° dip, 0° slip, pure north-south wave propagation) is shown in Figure 18. A third trace shows the difference of the two synthetics. A ripple in the third trace is evident, but the two synthetics match nearly perfectly. No set of traces thus far tested showed a mismatch $\gtrsim 1\%$ of the maximum trace amplitude, much smaller than the 10—40% misfit common to low-frequency source inversions. In return for this mismatch the user obtains considerable savings in computer CPU time and disk storage. Calculations taken to higher frequencies, however, may require the exact calculation with the Cholesky factors. Coupling between dissimilar modes for $f > 7$–8 mHz will likely depend strongly on shallow lateral structure in which relative density variation is high. Density variations of as much as 10—20% will significantly perturb the kinetic energy of hybrid mode singlets that correspond to surface waves traveling in the crust and uppermost mantle. This perturbation will be reflected in Cholesky factors that are noticeably distinct from the identity matrix.

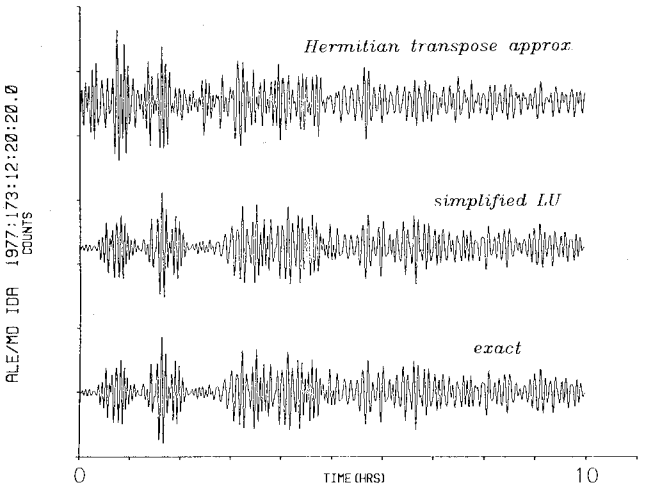

Fig. 17. Tonga-ALE seismograms for a strike-slip source oriented so as to maximize coupling effects. The complexity of the exact calculation is visually matched by the simplified LU algorithm synthetic. The Hermitian transpose approximation is clearly in error, with large noncausal waveforms.

7. SUMMARY

1. The investigation of free oscillation coupling on a nondissipative earth can be carried out with a variational formalism using a global basis of spherical earth oscillations in a narrow frequency band. The mechanical solution is found via the decomposition of a generalized matrix eigenvalue problem with Hermitian symmetry. The exact representation of interaction on a rotating earth requires a matrix equation that is quadratic in eigenfrequency ω. Coriolis interaction terms are grouped in a matrix linear in ω. If this linear dependence is removed by replacing ω with a fixed fiducial frequency $\hat{\omega}_0$, one needs only to solve a linear eigenvalue problem, affording a factor of 4—8 increase in computational speed, depending on computer architecture. Numerical experiments indicate that this approximation is adequate for modes with frequencies $\omega/2\pi \gtrsim 1$ mHz, as long as the relative frequency spread $(\Delta\omega)/(\hat{\omega}_0)$ is not large. The linearization of the problem results in the wrong sign for the second-order Coriolis contribution b^2m^2, which is significant for the gravest free oscillations, e.g., ${}_0S_2$. Calculations that include secular or nearly secular spherical earth modes must use the quadratic formulation.

2. The investigation of coupling using dissipative earth models requires the use of the more general Galerkin formalism. In this formalism, the Coriolis interaction and kinetic energy matrices retain Hermitian symmetry, but

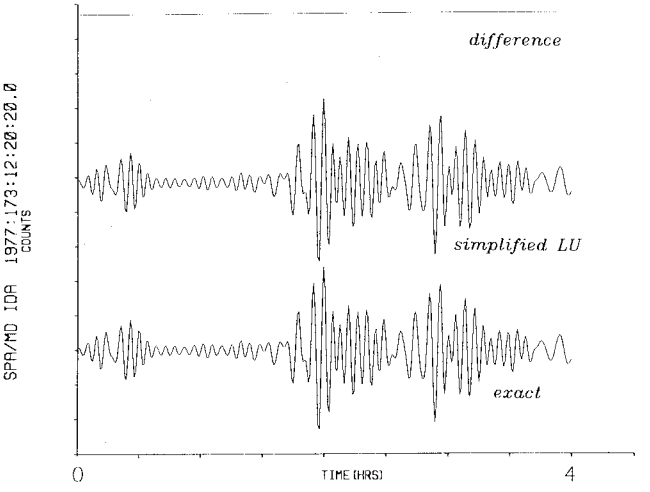

Fig. 18. Comparison of coupled-mode synthetics, for Tonga-SPA record of strike-slip event listed in text. The lower trace shows the exact calculation, composed, by virtue of the geometry, almost entirely of the spheroidal components of quasi-toroidal hybrid multiplets. The simplified LU synthetic is shown in the middle trace. The upper trace shows the difference of the two synthetic records. Four hours of seismic motion are shown.

the potential energy interaction matrix becomes general complex. The retention of symmetry in the former two matrices allows the problem to be solved via the COMQR2 EISPACK path, rather than the more general, but slower, LZ algorithm used by *Tanimoto and Bolt* [1983]. The loss of symmetry results in a large loss in computational speed relative to the fully Hermitian variational formalism. In some applications the increased precision is small relative to the increased effort. For example, if only coupling within an isolated multiplet is considered for an earth model that does not have lateral Q structure, the results are virtually identical to those gotten from a variational calculation in which the degenerate attenuation rate is appended to the hybrid eigenfrequencies. The effect of physical dispersion does not by itself break Hermitian symmetry in the interaction matrices, but its commonly assumed logarithmic dependence on frequency must be approximated by a truncated Taylor series about a chosen fiducial frequency $\hat{\omega}_0$ in order to retain a feasible numerical problem. The principal effect of physical dispersion on coupling is to widen slightly the frequency bandwidth across which coupled eigenfrequencies spread. This effect, however, is observationally negligible for the Q model of *Masters and Gilbert* [1983] and will likely be so for any reasonable Q model, barring the possible existence of significantly large, highly attenuative ($Q << 100$) regions in the earth.

3. The hybrid free oscillations of a dissipative earth model are represented by the right eigenvectors of the matrix interaction system. These eigenvectors are not necessarily orthogonal. The orthogonality of the degrees of vibrational freedom represented by these hybrid modes is retained by the fact that excitation calculations must use the left, or adjoint, eigenvectors of the matrix system, which form a vector space basis dual to that formed by the right eigenvectors. If the right eigenvectors are used instead for source excitation calculations, the resulting synthetic seismograms can be severely contaminated with spurious waveforms.

Acknowledgments. This work was supported by the National Science Foundation (NSF) grants EAR-82-18612 and EAR-84-09612, and IGPP-Lawrence Livermore National Laboratory grant PC831003. Guy Masters provided crucial software for handling IDA-type records and also contributed many useful comments. The assistance of R. C. Y. Chin and L. Thigpen greatly facilitated the use of the Livermore Laboratory computer. J. Park was partially supported by an NSF Graduate Fellowship in the early stages of this research.

REFERENCES

Akopyan, S. T., V. N. Zharkov, and V. M. Lyubimov, The dynamic shear modulus in the interior of the earth, *Dokl. Acad. Sci. USSR Earth Sci. Sect.*, Engl. Transl., *223*, 1–3, 1975.

Akopyan, S. T., V. N. Zharkov, and V. M. Lyubimov, Corrections to the eigenfrequencies of the earth due to the dynamic shear modulus, *Izv. Acad. Sci. USSR Phys. Solid Earth*, Engl. Transl., *12*, 625–630, 1976.

Buland, R., J. Berger, and F. Gilbert, Observations from the IDA network of attenuation and splitting during a recent earthquake, *Nature, 277*, 358–362, 1979.

Dahlen, F. A., The normal modes of a rotating, elliptical earth, *Geophys. J. R. Astron Soc., 16*, 329–367, 1968.

Dahlen, F. A., The normal modes of a rotating, elliptical earth, II, Near resonant multiplet coupling, *Geophys. J. R. Astron. Soc., 18*, 397–436, 1969.

Dahlen, F. A., Elastic dislocation theory for self-gravitating elastic configuration with an initial static stress field, II, Energy release, *Geophys. J. R. Astron. Soc., 31*, 469–484, 1973.

Dahlen, F. A., Excitation of the normal modes of a rotating earth model by an earthquake fault, *Geophys. J. R. Astron. Soc., 54*, 1–9, 1978.

Dahlen, F. A., The free oscillations of an anelastic aspherical earth, *Geophys. J. R. Astron. Soc., 66*, 1–22, 1981.

Dahlen, F. A., and R. V. Sailor, Rotational and elliptical splitting of the free oscillations of the earth, *Geophys. J. R. Astron. Soc., 58*, 609–623, 1979.

Dahlen, F. A., and M. L. Smith, The influence of rotation on the free oscillations of the earth, *Philos. Trans. R. Soc. London, Ser. A, 279*, 583–624, 1974.

Davis, J. P., Variation in apparent attenuation of the earth's normal modes due to lateral heterogeneity, *Geophys. Res. Lett., 12*, 141–143, 1985.

Dziewonski, A., and D. Anderson, A preliminary reference earth model, *Phys. Earth Planet. Inter., 25*, 297–356, 1981.

Edmonds, A. R., *Angular Momentum and Quantum Mechanics*, Princeton University Press, Princeton, N. J., 1960.

Garbow, B. S., J. M. Boyle, J. Dongarra, and C. B. Moler, *Matrix Eigensystem Routines—EISPACK Guide Extension*, Springer-Verlag, New York, 1977.

Gilbert, J. F., The diagonal sum rule and averaged eigenfrequencies, *Geophys. J. R. Astron. Soc., 23*, 125–128, 1971.

Gilbert, J. F., and A. M. Dziewonski, An application of normal mode theory to the retrieval of structural parameters and source mechanisms from seismic spectra, *Philos. Trans. R. Soc. London, Ser. A, 278*, 187–269, 1975.

Goldstein, H., *Classical Mechanics*, 2nd ed., 399 pp., Addison-Wesley, Reading, Mass., 1980.

Jordan, T. H., A procedure for estimating lateral variations from low-frequency eigenspectra data, *Geophys. J. R. Astron. Soc., 52*, 441–455, 1978.

Kawakatsu, H., and R. J. Geller, A new iterative method for finding the normal modes of a laterally heterogeneous body, *Geophys. Res. Lett., 8*, 1195–1197, 1981.

Lay, T., and H. Kamamori, Geometric effects of global lateral heterogeneity on long-period surface wave propagation, *J. Geophys. Res., 90*, 605–621, 1985.

Liu, H.-P., D. L. Anderson, and H. Kanamori, Velocity dispersion due to anelasticity; implications for seismology and mantle composition, *Geophys. J. R. Astron. Soc., 47*, 41–58, 1976.

Luh, P. C., The normal modes of the rotating self-gravitating inhomogeneous earth, *Geophys. J. R. Astron. Soc., 38*, 187–224, 1974.

Madariaga, R. I., Free oscillations of the laterally inhomogeneous earth, Ph.D. thesis, 105 pp., Mass. Inst. of Technol., Cambridge, 1971.

Marchuk, G. I., *Methods of Numerical Mathematics*, Springer-Verlag, New York, 1975.

Masters, T. G., Observational constraints on the chemical and thermal structure of the earth's deep interior, *Geophys. J. R. Astron. Soc., 57*, 507–534, 1979.

Masters, G., and F. Gilbert, Structure of the inner core inferred from observations of its spheroidal shear modes, *Geophys. Res. Lett., 8*, 569–571, 1981.

Masters, G., and F. Gilbert, Attenuation in the earth at low frequencies, *Philos. Trans. R. Soc. London, Ser. A, 308*, 479–522, 1983.

Masters, G., T. H. Jordan, P. G. Silver, and F. Gilbert, Aspherical earth structure from fundamental spheroidal-mode data, *Nature, 298*, 609–613, 1982.

Masters, G., J. Park, and F. Gilbert, Observations of coupled spheroidal and toroidal modes, *J. Geophys. Res., 88*, 10,285–10,298, 1983.

Moiseiwitsch, B. L., *Variational Principles*, John Wiley, New York, 1966.

Morris, S. P., and R. J. Geller, Toroidal modes of a simple laterally heterogeneous sphere, *Bull. Seismol. Soc. Am., 72*, 1155–1166, 1982.

Nakanishi, I., and D. L. Anderson, Measurements of mantle wave velocities and inversion for lateral heterogeneity and anisotropy, 1, Analysis of great-circle phase velocities, *J. Geophys. Res., 88*, 10–267, 1983.

Nakanishi, I., and D. L. Anderson, Measurements of mantle wave velocities and inversion for lateral heterogeneity and anisotropy.

II. Analysis by the single station method, *Geophys. J. R. Astron. Soc., 78*, 573–617, 1984.
Okal, E. A., The effect of intrinsic ocean upper-mantle heterogeneity on regionalization of long-period Rayleigh-wave phase velocities, *Geophys. J. R. Astron. Soc., 49*, 357–370, 1977.
Park, J., Applications of the Galerkin formalism in the coupling of the earth's free oscillations, Ph.D. Thesis, Univ. Calif., San Diego, La Jolla, 1985.
Park, J., Synthetic seismograms from coupled free oscillations: The effects of lateral structure and rotation, *J. Geophys. Res.*, in press, 1986.
Rydelek, P. A., and L. Knopoff, Spectral analysis of gapped data: search for ${}_1S_1$ of the south pole, *J. Geophys. Res., 89*, 1899–1902, 1984.
Silver, P. G., and T. H. Jordan, Fundamental spheroidal mode observations of aspherical heterogeneity, *Geophys. J. R. Astron. Soc., 64*, 605–634, 1981.
Sipkin, S. A., and T. H. Jordan, Multiple *ScS* times in the western Pacific: Implications for mantle heterogeneity, *J. Geophys. Res., 89*, 853–861, 1980.
Smith, M. L., and F. A. Dahlen, The period and Q of the Chandler wobble, *Geophys. J. R. Astron. Soc., 64*, 223–282, 1981.
Sommerfeld, A., *Mechanics, Lectures on Physics*, vol. I, 289 pp., Academic, Orlando, Fla., 1952.
Stifler, J. F., and B. A. Bolt, Eigenvibrations of laterally inhomogeneous earth models, *Geophys. J. R. Astron. Soc., 64*, 201–221, 1981.
Tanimoto, T., Waveform inversion of mantle Love waves: The Born seismogram approach, *Geophys. J. R. Astron. Soc., 78*, 641–660, 1984.
Tanimoto, T., and D. L. Anderson, Lateral heterogeneity and azimuthal anisotropy of the upper mantle: Love and Rayleigh waves 100–250 s, *J. Geophys. Res., 90*, 1842–1858, 1985.
Tanimoto, T., and B. A. Bolt, Coupling of torsional modes in the earth, *Geophys. J. R. Astron. Soc., 74*, 83–96, 1983.
Wong, Y. K., and J. H. Woodhouse, Ray theory for surface waves on a sphere (abstract), *Eos Trans. AGU, 64*, 260, 1983.
Woodhouse, J. H., On Rayleigh's principle, *Geophys. J. R. Astron. Soc., 46*, 11–22, 1976.
Woodhouse, J. H., The coupling and attenuation of nearly resonant multiplets in the earth's free oscillation spectrum, *Geophys. J. R. Astron. Soc., 61*, 261–283, 1980.
Woodhouse, J. H., and F. A. Dahlen, The effect of a general aspherical perturbation on the free oscillations of the earth, *Geophys. J. R. Astron. Soc., 53*, 335–354, 1978.
Woodhouse, J. H., and A. M. Dziewonski, Mapping of the upper mantle: Three-dimensional modeling of earth structure by inversion of seismic waveforms, *J. Geophys. Res., 89*, 5953–5986, 1984.
Woodhouse, J. H., and T. P. Girnius, Surface waves and free oscillations in a regionalized earth model, *Geophys. J. R. Astron. Soc., 68*, 653–673, 1982.
Zharkov, B. N., and V. M. Lyubimov, Torsional oscillations of a spherically asymmetrical model of the earth, *Izv. Acad. Sci. USSR Phys. Solid Earth*, Engl. Transl., no. 2, 71–76, 1970*a*.
Zharkov, B. N., and V. M. Lyubimov, Theory of spheroidal vibrations for a spherically asymmetrical model of the earth, *Izv. Acad. Sci. USSR Phys. Solid Earth*, Engl. Transl., no. 10, 613–618, 1970*b*.

F. Gilbert, Institute of Geophysics and Planetary Physics, Scripps Institution of Oceanography, University of California, San Diego, La Jolla, CA 92093.
J. Park, Geophysical Fluid Dynamics Program, Princeton University, P.O. Box 308, Princeton, NJ 08544.

(Received February 8, 1985;
revised October 7, 1985;
accepted January 29, 1986.)